



Observations of Diurnal Variability under the Cirrus Canopy of Typhoon Kong-rey (2018)

BENJAMIN C. TRABING^a AND MICHAEL M. BELL^a

^aColorado State University, Fort Collins, Colorado

(Manuscript received 5 October 2020, in final form 28 May 2021)

ABSTRACT: A growing body of work has documented the existence of diurnal oscillations in the tropical cyclone outflow layer. These diurnal pulses have been examined primarily using satellites or numerical models, and detailed full tropospheric observations or case study analyses of diurnal pulses are lacking. Questions remain on the vertical extent of diurnal pulses and whether diurnal pulses are coupled to convective bands or constrained to the outflow layer. During the Propagation of Intraseasonal Tropical Oscillations (PISTON) field campaign, diurnal oscillations in the upper-level clouds were observed during Typhoon Kong-rey's (2018) rapid intensification. Over a 3.5-day period where a broad distribution of cold upper-level clouds was overhead, detailed observations of Typhoon Kong-rey's rainbands show that convection had reduced echo tops but enhanced reflectivity and differential reflectivity aloft compared to other observations during PISTON. Shortwave heating in the upper levels increased the stability profile in an overall favorable thermodynamic environment for convection during the day, which could help to explain the diurnal differences in convective structure. Under the cirrus canopy, nocturnal convection was deeper and daytime convection shallower in contrast to the rest of the PISTON dataset. Diurnal oscillations in the brightness temperatures were found to be coupled to radially outward propagating convective rainbands that were preceded ~6 h by outflow jets. The cooling pulses occurred earlier than found in previous studies. The pulses were asymmetric spatially, which is likely due to a combination of the vertical wind shear and storm intensity.

KEYWORDS: Rainbands; Diurnal effects; Tropical cyclones; In situ atmospheric observations; Radars/Radar observations

1. Introduction

Modeling experiments have shown that radiation plays an important role in the evolution of tropical cyclones (TCs) and their forecasts (Sundqvist 1970; Hobgood 1986; Craig 1996; Nicholls 2015; Fovell et al. 2016; Navarro et al. 2017; Trabing et al. 2019; Ruppert and O'Neill 2019). Including radiation in models often leads to increases in rates of tropical cyclogenesis and mitigates the negative effects of vertical wind shear allowing intensification to occur sooner (Melhauser and Zhang 2014; Nicholls 2015; Rios-Berrios 2020; Smith et al. 2020; Ruppert et al. 2020). TC intensity change and inner-core structure are sensitive to the cloud microphysics, and the interactions between the microphysics and radiation schemes can lead to forecast errors in the tracks of TCs and differences in storm size that affect wind radii forecasts (Zhu and Zhang 2006; Fovell et al. 2010; Bu et al. 2014; Fovell et al. 2016). Improvements in TC forecasting may require improved understanding and representation of cloud-radiative processes in forecast models through observational analysis and verification (Fovell et al. 2016). In the current study we aim to improve the understanding of cloud-radiative processes through analysis of field observations of the diurnal cycle of convection in rainbands under the cirrus canopy of an intensifying tropical cyclone.

Past modeling studies of idealized tropical cyclones have shown that the diurnal cycle of solar radiation affects the

distribution of rainband convection. Zhou et al. (2016) found that solar radiation impacts rainband convection by modulating the strength of cold pools. Tang et al. (2017) found that solar heating at upper levels is important for stabilizing the moat region of Hurricane Edouard (2014) simulations, which causes convection outside of the eyewall to develop at larger radii. The location of the primary rainbands was critical for the accurate simulation of a secondary eyewall formation in Hurricane Edouard. Trabing and Bell (2021) found that shortwave heating in the upper levels of rainband convection is responsible for weakening the diabatic heating profiles of convective clouds during the day and can modify the timing of secondary eyewall formation. Kossin and DeMaria (2016) showed that large intensity forecast errors can sometimes be attributed to the lack of accurate secondary eyewall prediction. However, it has also been noted that a cycle of convection on diurnal time scales in simulated tropical cyclones might not require shortwave radiation. Li and Wang (2012) showed a 22–26-h cycle of inner-core rainbands associated with the boundary layer recovery timing of convective downdrafts and consumption of convective available potential energy (CAPE). Observations of the diurnal cycle of convective rainbands associated with tropical cyclones are lacking, but are needed to verify the analyses of idealized numerical model studies.

It is well established that the diurnal cycle of precipitation over the ocean in the tropics reaches a peak in the early morning hours (e.g., Gray and Jacobson 1977; Steranka et al. 1977; Bowman and Fowler 2015). The convection in the inner core of TCs has consistently been shown to be stronger in the overnight hours preceding the peak in rainfall (Leppert and

Corresponding author: Benjamin Trabing, btrabing@colostate.edu

Cecil 2016; Navarro and Hakim 2016). Inner-core deep convection in the overnight hours is also related to higher frequency of occurrences and higher rates of intensification for global TCs (Wu et al. 2020). Some studies have suggested that the cirrus canopy is formed when deep inner-core convection penetrates the stable outflow layer and spreads radially, meaning that the cirrus canopy formation and fluctuations in thickness/altitude should therefore lag the diurnal cycle of convection (Merritt and Wexler 1967; Duran and Molinari 2016; Houze 2010). Studies have shown that the areal extent of the cirrus canopy is minimized in the early morning and maximized in the afternoon, which supports the lagged response from the diurnal cycle of inner-core convection (Muramatsu 1983; Steranka et al. 1977; Wu and Ruan 2016). Although cirrus clouds above TCs are thought to be generated by the strong inner-core convection and advected outward, it is unclear how much rainband convection contributes to the volume of ice in the cirrus canopy. Deep convection in the outer core and in the TC rainbands have been shown to have a secondary peak in rainfall in afternoon (Leppert and Cecil 2016), which could potentially contribute to the expansion of the cirrus canopy in the afternoon. The diurnal oscillations in the areal extent and temperature of the cirrus canopy over tropical cyclones is important to consider due to the effect on the Dvorak pattern-recognition technique for objectively estimating intensity (Muramatsu 1983; Dunion et al. 2014).

In addition to having a diurnal cycle of areal extent, cirrus clouds have been suggested to modify the diurnal cycle of deep convective clouds. Using observations from both microwave and infrared satellites, Hong et al. (2006) found a two hour delay in the diurnal cycle of convection due to cirrus clouds and an enhancement of the diurnal variations in the blended 11- μm areal fraction of 210 K (cloud tops above 13.5 km) deep convective clouds in non-TC environments. One mechanism by which the cirrus canopy can modulate the diurnal cycle of convection is through modification of the location and magnitude of shortwave and longwave radiative tendencies in the atmosphere. A thin cirrus canopy would result in more reflection of shortwave radiation, while a thicker canopy would result in increased absorption within the cloud, and both would reduce the magnitude of shortwave radiation available to warm the ocean surface. Using an idealized linear model, Evans and Nolan (2019) showed that direct radiative heating in the cirrus canopy may be responsible for generating gravity waves that can propagate away from the tropical cyclone center and throughout the depth of the troposphere. The radiative heating/cooling anomalies in the cirrus canopy can also change the upper-level stability and induce anomalies on the secondary circulation of the TC which could feedback on the strength of convection (Duran and Molinari 2016; Navarro and Hakim 2016; Navarro et al. 2017).

The diurnal cycle of tropical cyclone rainband convection, and any impacts from the cirrus canopy, may be complicated by the existence of outward propagating rings of cold infrared (IR) brightness temperatures. A growing body of work has documented these propagating cold rings within the outflow layers of mature tropical cyclones, referred to hereafter as diurnal pulses or cooling pulses (Dunion et al. 2014). Although

diurnal pulses were initially discovered in strong tropical cyclones, Ditchek et al. (2019a) found that diurnal pulses occur in 80% of major hurricane days, 64% of minor hurricane days, and 46% of tropical storm days in the Atlantic from 1982 to 2017. Their study also shows variability in the pulses based on the thermodynamic environment and documents the occurrence of warming pulses. Knaff et al. (2019) examined all Northern Hemisphere storms from 2005 to 2015 and found that 61% of major hurricanes, 54% of hurricanes, and 45% tropical storms have a moderate to strong diurnal signal. Knaff et al. (2019) suggests that the prevalence of diurnal oscillations in the brightness temperatures of tropical cyclones is affected by factors controlling the azimuthal symmetry, such as the vertical wind shear, intensity, and storm motion. The importance of a favorable environment for convection, particularly the upper-level relative humidity, has been suggested by multiple recent studies to be also important for diurnal pulses (Ditchek et al. 2019a; Knaff et al. 2019; Ditchek et al. 2019b). It is unclear, however, what factors contribute to variations in the time of initiation of diurnal pulses and why weak tropical cyclones may exhibit diurnal pulses with a weaker secondary circulation.

The underlying mechanisms that govern the initiation and propagation of diurnal pulses are an active area of research. Dunion et al. (2014) noted several initiation mechanisms that could be at play including convective coupled gravity waves, cloudy-clear sky radiative disequilibrium (Gray and Jacobson 1977), direct radiative-convective interactions (Xu and Randall 1995), radiatively reduced outflow resistance (Mecikalski and Tripoli 1998), and/or a seeder-feeder mechanism from falling ice crystals (Houze et al. 1981). Ditchek et al. (2020) further noted that diurnal pulses may be initiated by inner rainbands that become reinvigorated after propagating radially outward into thermodynamically favorable environments. It is unclear whether all diurnal pulses are coupled with deep convection, or if the features are driven by processes solely in the outflow layer. Ditchek et al. (2019b) used ground-based lightning observations to show that diurnal pulses are electrically active ~61% of the time. The correlation of cooling pulses with lightning suggests a coupling with deep convection strong enough to generate charge to produce lightning in most cases; however, it is unclear if the electrically inactive pulses are cirrus canopy features or coupled with relatively weaker convection. The recent modeling study by Dunion et al. (2019) suggests that diurnal pulses can be characterized by outwardly moving squall lines with associated gust fronts. Dunion et al. (2019) showed that the outward moving squall lines tend to decrease in height with increasing radius because of increased static stability due to shortwave warming during the day. Ditchek et al. (2020) used radar, satellite and lightning observations in Hurricane Harvey (2017) to provide further support that electrically active cooling pulses are coupled with squall lines. One hypothesis suggested by O'Neill et al. (2017) is that the diurnal pulses are linked to gravity waves that may be initiated by an enhancement of convection in the inner core that becomes coupled with convection as it moves radially outward. The mechanisms controlling how cooling pulses become coupled to outward propagating squall lines or why

they are consistently tied to the diurnal cycle are still open questions.

Diurnal pulses have been examined primarily using satellites and numerical models, but multidimensional observations of diurnal pulses are lacking. During the Propagation of Intraseasonal Tropical Oscillations (PISTON) field campaign, diurnal pulses in the infrared brightness temperatures of Typhoon Kong-rey were evident. The thermodynamic and kinematic properties of the environment of Typhoon Kong-rey (2018) were sampled during PISTON over multiple days with ship-borne observing systems, which will be discussed in section 2. These observations provide a novel look at convective and stratiform cloud properties of the TC rainbands and environment under a cirrus canopy in which multiple diurnal oscillations in the brightness temperatures are found. Observations of diurnal pulses from below the cloud layer in a marine environment have not been previously examined to the authors' knowledge. Using a suite of observations, this study seeks to understand the diurnal variability of convective and stratiform precipitation under a broad cirrus canopy and explore the characteristics of diurnal pulses from a new perspective. This study provides new insight into the complex interactions between radiation and tropical cyclone rainbands that can be used to validate future modeling studies and improve forecasts. The observations from PISTON will help us address the following science questions:

- How does the diurnal cycle of convective and stratiform precipitation vary under the cirrus canopy of Typhoon Kong-rey?
- What role does the thermodynamic environment play in the variability of the observed rainband convection?
- Are the diurnal pulses in Typhoon Kong-rey convectively coupled and consistent with previous modeling studies?

To answer the questions posed above, the study is organized as follows. Section 2 will detail the observations collected during PISTON that will be used in this study. Section 3 will show how convective and stratiform clouds varied while under the cirrus canopy of Typhoon Kong-rey and with the diurnal cycle. The observations of the outward propagating cold rings, which will be herein referred to as “cooling pulses” will be shown in section 4. The results of this study will be discussed in section 5.

2. Data and methods

During the PISTON field campaign in 2018, observations from two cruises of the R/V *Thomas G. Thompson* were collected in the western North Pacific from mid-August to mid-October. Although the original goal of the experiment was to observe the ocean and atmospheric response to the boreal summer intraseasonal oscillation (BSISO), persistent typhoon activity near the area of operations comprised most of the variability in the observed ocean and atmosphere states during the project period (Sobel et al. 2021). We make use of the novel observations collected during the PISTON field campaign to investigate the diurnal cycle of convection within tropical cyclone rainbands in detail. The focus of this study will be on

Typhoon Kong-rey (WP302018), which was a well-observed typhoon during the experiment between September 29 and October 3. Typhoon Kong-rey slowly tracked near the R/V *Thomas G. Thompson*, allowing detailed observations of the convective rainbands to be collected under a broad cirrus canopy. We leverage space-based and ship-borne observations in this detailed case study of Typhoon Kong-rey.

The track and intensity of Typhoon Kong-rey in this study are taken from the best track database produced by the Joint Typhoon Warning Center (JTWC). The track and intensity evolution of Typhoon Kong-rey from the JTWC are shown in Fig. 1. The pink shading in Fig. 1a highlights the 2-day period that the R/V *Thomas G. Thompson* was within ~500 km of the center of Typhoon Kong-rey. During these two days as shown with the pink lines in Fig. 1b, Typhoon Kong-rey underwent rapid intensification (RI) from a tropical storm to a category 5 on the Saffir–Simpson wind speed scale (Schott et al. 2012). It should be noted that observations outside the shaded region were still being collected but were at further storm relative radii and less constrained by TC dynamics to some degree. The period of interest in this study will span from ~0900 UTC 29 September to ~2100 UTC 2 October (~1800 LST 29 September–~0600 LST 3 October) during which a persistent cirrus canopy was present directly above the R/V *Thomas G. Thompson* as will be shown later. We use a constant 9-h offset to coordinate with local solar time (LST). Kong-rey tracked to the northeast of the ship, which was at a relatively fixed location over the entire time period of interest. After reaching peak intensity, Kong-rey began to weaken due to the effects of cold water which was upwelled after Super Typhoon Trami stalled days earlier. Overall, observations of Typhoon Kong-rey's rainbands under anvil-like cirrus clouds were collected over a period of three and a half days.

Over the entire PISTON field campaign, the thermodynamic environment was sampled every three hours with 375 soundings released in total. The large number of radiosondes over the course of the field campaign allows for a good comparison between the observations surrounding Typhoon Kong-rey and the PISTON mean environment. While the ship was located within 500 km of the 6-hourly center of Typhoon Kong-rey (shading in Fig. 1a), 17 consecutive radiosondes were launched. A total of 33 radiosondes were launched between 1500 LST 29 September and 0900 LST 3 October while a broad distribution of upper-level clouds were prevalent overhead. Radiosondes were both objectively and subjectively quality controlled following the procedures of Ciesielski et al. (2012). In addition to the soundings, we incorporate observations from a radiometer measuring downward solar fluxes and a high spectral resolution lidar (HSRL) which is used to estimate cloud base height. We use the HSRL backscatter at 10-min temporal and 60-m vertical intervals. Together, these instruments are able to provide insights into the diurnal changes in the thermodynamics.

An important tool for this analysis is the new Sea-Going Polarimetric (SEA-POL) radar. SEA-POL is the first polarimetric C-band weather radar designed to deploy on research ships for the U.S. research community (Rutledge et al. 2019). SEA-POL allows us to examine the variability of precipitating

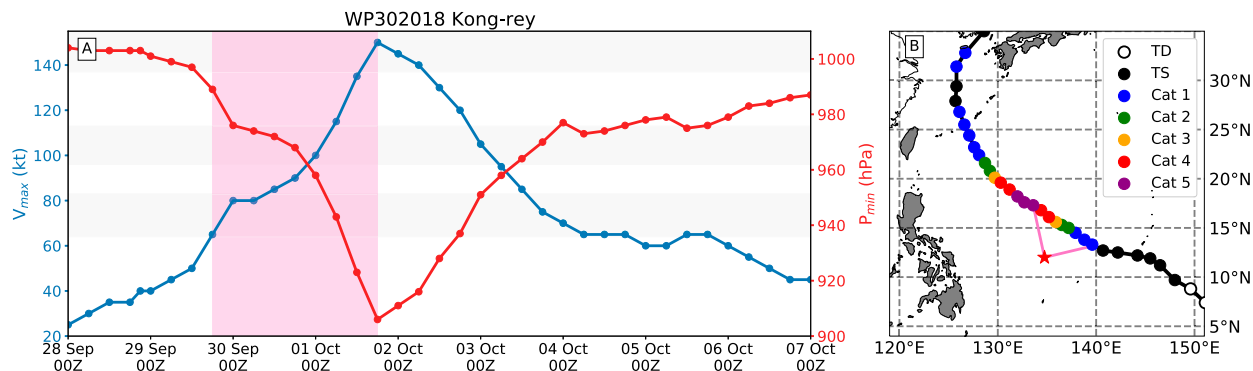


FIG. 1. (a) The intensity evolution of Typhoon Kong-rey with 1-min sustained maximum wind speeds (blue curve) and minimum central pressure (red curve) from the JTWC best track. The pink shading indicates the times where the R/V *Thomas G. Thompson* was within 500 km of the tropical cyclone center during rapid intensification. (b) The 6-hourly track of Typhoon Kong-rey's center is shown colored by the Saffir–Simpson wind speed category based on maximum surface wind speeds. The red star indicates the general position of the R/V *Thomas G. Thompson*. The pink lines connecting the ship and TC track indicate the beginning and end of the red shaded region in (a).

cloud distributions during PISTON. The radar has a range of 120 km and completes full volume scans every 12 min with scanning levels modified based on the proximity of high-dBZ echoes to the radar. SEA-POL has a limited 240° field of view relative to the ship direction because its position on the forward “02” deck is below the bridge. Since the radar does not have a complete 360° field of view, changes in the ship direction can lead to changes in the observed distribution of clouds. Despite the limited field of view, SEA-POL provides a large enough sample size for good comparisons of convective characteristics in different environments. Quality control procedures for SEA-POL data includes a correction for ship motion, beam attenuation, and the removal of nonmeteorological clutter (Rutledge et al. 2019).

The key SEA-POL radar moments that will be evaluated in this study are the reflectivity and the differential reflectivity (ZDR). Reflectivity is the backscattered power in units of dBZ which provides information on the size and number concentration of particles. ZDR is the difference between the horizontally and vertically polarized reflectivity factors in units of dB, which provides information on the shape of the particles. SEA-POL data are regressed to a Cartesian grid using the tools in the Lidar Radar Open Software Environment (LROSE; Bell et al. 2019). A convective-stratiform partition algorithm is employed on the gridded reflectivity data to objectively identify areas of convective precipitation, stratiform precipitation, and clouds with weak echoes. We use the convective-stratiform partition developed by Steiner et al. (1995) and upgraded by Yuter and Houze (1997), which identifies regions based on reflectivity thresholds and the horizontal reflectivity gradient at 2 km. Sensitivity tests indicate the Yuter and Houze (1997) algorithm provides similar results compared to Powell et al. (2016), with less rain-type categories but a more coherent time series. The focus of this work will be on both the convective and stratiform components of the tropical cyclone outer-core rainbands, which have been shown to be important in affecting tropical cyclone intensity change (Wang and Tan 2020).

The observations near the surface from the R/V *Thomas G. Thompson* were supplemented by the global observing

system. We examine cloud top temperatures in the infrared (IR) and 6-h IR brightness temperature differences from the *Himawari-8* Advanced Himawari Imager to identify the presence of cold upper level clouds within the cirrus canopy and variations therein associated with diurnal pulses. Infrared bands at 10.4, 11.2, and 12.3 μm were analyzed, but here we focus primarily on the 10.4- μm infrared band. At cold temperatures, the difference between the infrared bands is small and the results shown are not sensitive to the band chosen. Passive satellite imagery from the Tropical Cyclone Precipitation, Infrared, Microwave, and Environmental Dataset (TC PRIMED; Razin et al. 2021) are used to observe cloud structure below the cirrus clouds when available. The 89–91.6-GHz channels from SSMIS and GMI satellites identify deep convective clouds associated with Typhoon Kong-rey’s rainbands which generated large distributions of ice species. The microwave imagery provides only snapshots at irregular time intervals and will be used to evaluate convective organization near Typhoon Kong-rey’s center where ship-borne observations are impossible.

3. Rainbands under the cirrus canopy

We first document the distribution of cloud top IR brightness temperatures to provide context of the cirrus canopy in the PISTON domain. Figure 2 shows the evolution of the distribution of brightness temperatures in a 120 km \times 120 km area centered on the location of the R/V *Thomas G. Thompson* during the time period surrounding Typhoon Kong-rey. The passage of upper-level cirrus clouds over the ship first occurs around 2100 LST September 29 when the distribution of brightness temperatures shifts from warm IR temperatures between 280 and 300 K to mostly cold clouds between 210 and 230 K. From 2100 LST 29 September to 0300 LST 3 October the distribution of cloud top temperatures are predominantly between 210 and 230 K suggesting the presence of clouds reaching altitudes of 10–14 km over the entirety of \sim 3.5 days. The present study focuses on this time frame (2100 LST 29 September–0300 LST 3 October), with the continuous

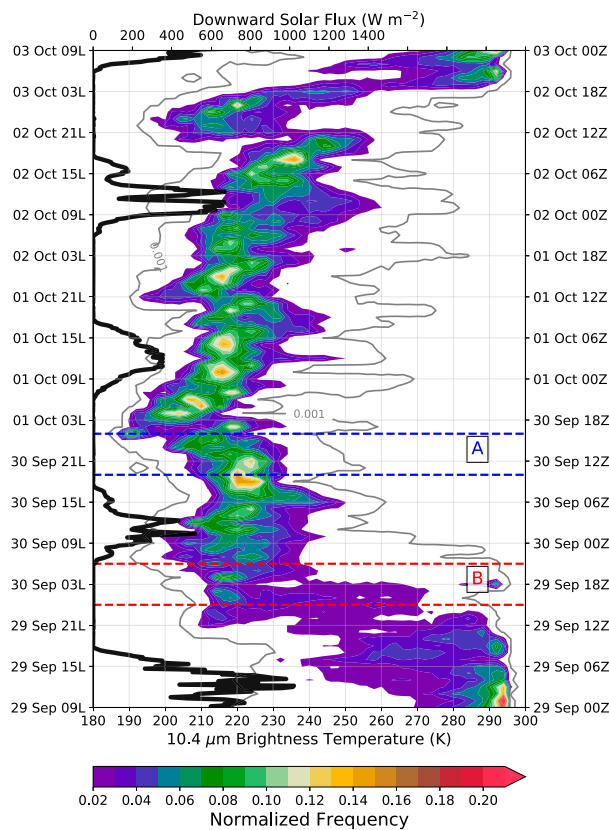


FIG. 2. The temporal evolution of the distribution of 10.4- μm brightness temperatures from *Himawari-8* over a 120 km \times 120 km box centered over the R/V *Thomas G. Thompson*. Brightness temperatures are binned at 1-K increments and normalized by the number of pixels in the box. The gray line is the 0.001 frequency contour. The black line is the downward solar flux observed on the R/V *Thomas G. Thompson* during the time period using the top abscissa. The blue and red dashed lines are the time periods of 6-h brightness temperature differences corresponding to the TC centered imagery in Figs. 11a and 11b.

presence of a cirrus canopy and anvil cirrus. The upper-level cloud distribution shown is a combination of cirrus emanating from Typhoon Kong-rey's inner-core convection and some contribution from the convective rainbands.

In addition to the continuous presence of upper-level clouds during the Kong-rey time period, there is considerable variability in the distribution of brightness temperatures. For coordination with the diurnal cycle, the thick black line in Fig. 2 shows the measured solar downward flux from the ship-based radiometer. The downward solar flux is reduced compared to clear sky days due to the absorption and reflection by the clouds above. The measured downward solar flux over the three cloudy days never exceeded 700 W m^{-2} with peak measured fluxes on 1 October reaching only 400 W m^{-2} . The peak downward solar fluxes during clear skies reached around 1200 W m^{-2} during PISTON, suggesting that the clouds and atmospheric gases scattered and absorbed between 40% and 70% of the incoming solar energy. The coldest brightness

temperatures ($\leq 200 \text{ K}$) are primarily found at night or in the early morning times, likely associated with deep convection and consistent with past studies. During the daytime, times from ~ 0600 to 1800 LST (~ 2100 –0900 UTC), there is a noticeable shift in the peak of the brightness temperature distributions to warmer temperatures. The presence of warmer brightness temperatures in the afternoon away from the storm center is consistent with previous studies such as Steranka et al. (1977) and Wu and Ruan (2016). Although the colder brightness temperatures at night and warmer brightness temperatures during the day are consistent with the diurnal cycle of convection in the oceanic tropics, the TC circulation complicates the interpretation. It is unclear how much of the changes in brightness temperatures are a response to ice generated by deep convection in the inner core of the TC that is ejected radially outward in the outflow layer, or due to the diurnal cycle of convection in the rainbands. We note here that there are two periods where outward propagating diurnal pulses are observed at the ship, denoted by the blue and red dashed lines, which will be discussed in the next section.

To analyze differences in the clouds under Kong-rey's cirrus canopy, we analyze contoured frequency by altitude diagrams (CFADs) of the reflectivity and differential reflectivity measured by SEA-POL. Using the convective–stratiform partition, we compare the reflectivity of convective and stratiform precipitation features associated with Typhoon Kong-rey to the full distribution of convective and stratiform clouds during the PISTON field campaign in Fig. 3. Due to the differences in sample size, the CFADs are normalized by the total number of samples observed to allow for better comparisons between the time periods. To first order, the overall CFADs of the full PISTON distribution and the time period of interest under the cirrus and widespread clouds in the convective (Figs. 3a,b) and stratiform (Figs. 3d,e) profiles look quite similar. The CFADs for ZDR shown in Fig. 4 also show few first-order differences.

The distributions suggest broad similarity between the convection observed near the TC and typical convection observed during PISTON, but some differences are apparent when subtracting the normalized CFADs as shown in Figs. 3c and 4c and 3f and 4f. In both cases, the peak height of convective and stratiform clouds around Typhoon Kong-rey is lower with fewer reflectivity echoes reaching altitudes above 14 km. There are two potential reasons for this difference. One explanation is that the upper levels have been stabilized through radiative cooling above the cloud and radiative warming within the cloud (Duran and Molinari 2019). It is also possible that an upper-level constraint can be attributed to the dynamics of the TC, as cloud heights are constrained vertically by the layer of strong outflow from the primary TC eyewall (Houze 2010). Given that the convective profiles are observed in a range of radii from 200 to 700 km from Kong-rey, there is likely a combination of the two constraints at play. Even though the peak altitudes are reduced, there is an overall increase in the frequency of convective and stratiform clouds reaching 8–10 km with 20-dBZ reflectivity echoes. Corresponding to the increase in reflectivity, there is also an increase in the

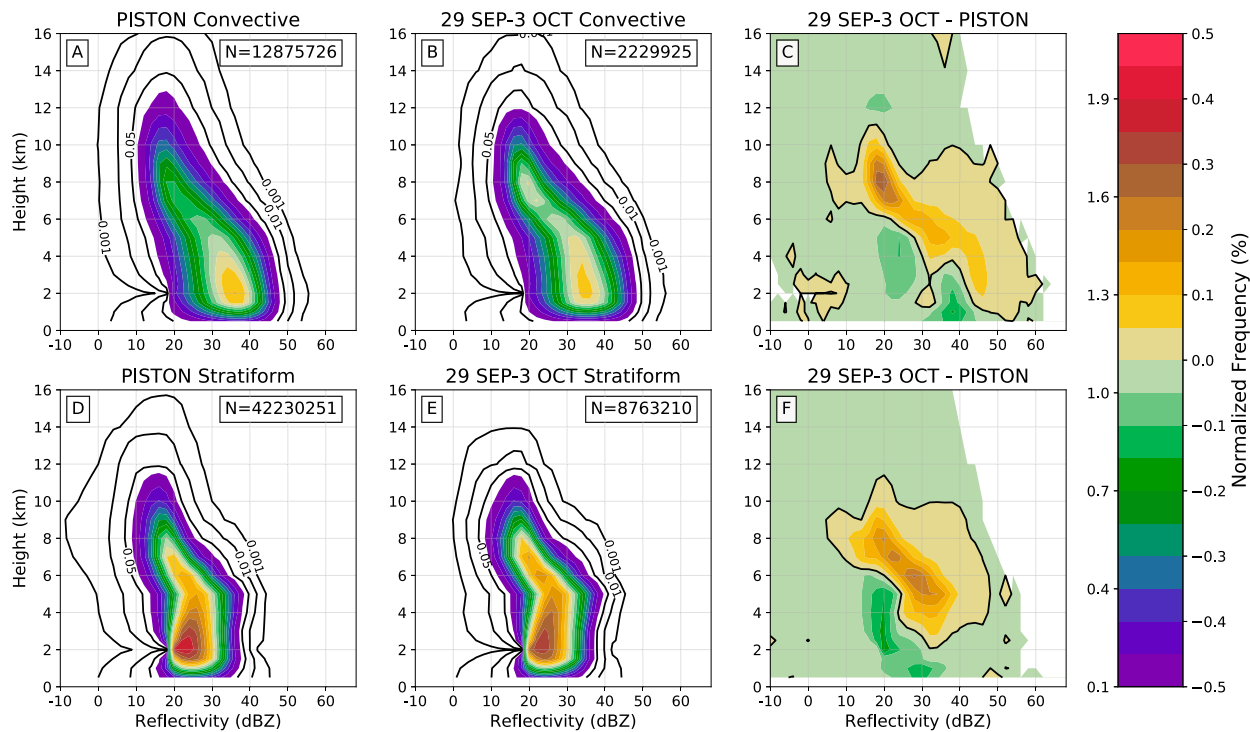


FIG. 3. CFADs for all points defined as convective within the range of SEA-POL (a) during the PISTON field campaign and (b) over just the time period of interest from 29 Sep to 3 Oct. CFADs for stratiform defined echoes (d) over PISTON and (e) the time period of interest. The CFADs are normalized by the total number of echoes observed in each category, which is shown by N , to limit differences due to sampling. The differences between the time period of interest and all of PISTON for (c) convective echoes and (f) stratiform echoes. The zero line is highlighted with the black line, and bins with no echoes are whited out. CFADs are binned every 1 km at 2-dBZ intervals. Total distributions use the left side of the color bar with differences using the right side.

ZDR values from 0.5 to 1.0 dB, suggesting a slight increase in the median size of the hydrometeors (Fig. 4). There appears to be a shift in the distribution of reflectivity echoes toward larger values under the cirrus canopy around, and below, the melting level (~ 5 km). The shift in the distribution suggests that convection was able to more consistently grow to greater heights and produce both larger, as suggested by the greater ZDR, and higher concentrations of water droplets and ice/snow crystals. The differences in strength of convection are likely not tied directly to the cirrus canopy, but suggest a more favorable environment for convection when the cirrus canopy is present.

To investigate the diurnal cycle of convection in the outer core convection, we analyze the CFADs of outer rainband precipitation in a similar manner as Fig. 3 but with profiles separated into day and night categories. Consistent with Figs. 3 and 4, there are no major differences between the overall patterns of the normalized CFADs in Fig. 5 but there are some quantitative differences in the distributions. The PISTON-wide diurnal difference in convection (Fig. 5c) shows weak contrast overall, suggesting small but still noticeable differences in convective intensity due to radiation during the two months of observations. Figure 5c indicates that convection during the daytime hours has a more peaked distribution at upper levels with slightly higher reflectivity values. Interestingly, the PISTON wide day–night difference

does not suggest that nocturnal convection is stronger, despite the higher relative humidity from longwave cooling normally found at night (Melhauser and Zhang 2014). Instead, a slight daytime enhancement of reflectivities suggests that the presence of diurnal warm layers, which are prevalent in clear sky low-wind regimes, likely played a larger role in enhancing convection (Bellenger et al. 2010; Thompson et al. 2019). Hughes et al. (2020) showed that during the second cruise of PISTON, 12 of the 24 days with SurfOtter observations had diurnal warm layers present. The stratiform CFADs in Fig. 6 show similar results with a daytime enhancement of larger reflectivities at nearly all levels in the PISTON-wide CFAD. Rowe et al. (2019) similarly found a daytime enhancement of precipitation from wide convective core and broad stratiform regions on longer time scales associated with an active phase of the Madden-Julian oscillation, which demonstrates that the large scale conditions can modulate the diurnal cycle.

During the time period of interest where the cirrus canopy of Typhoon Kong-rey is present, the differences between nighttime and daytime convection are more pronounced (Fig. 5f). The stronger differences in reflectivity suggest that the diurnal cycle of convection was modified in the TC environment, potentially by the cirrus canopy and upper-level clouds of various optical depths. We have normalized the data by the number of events; however, the possibility that the smaller sample size is

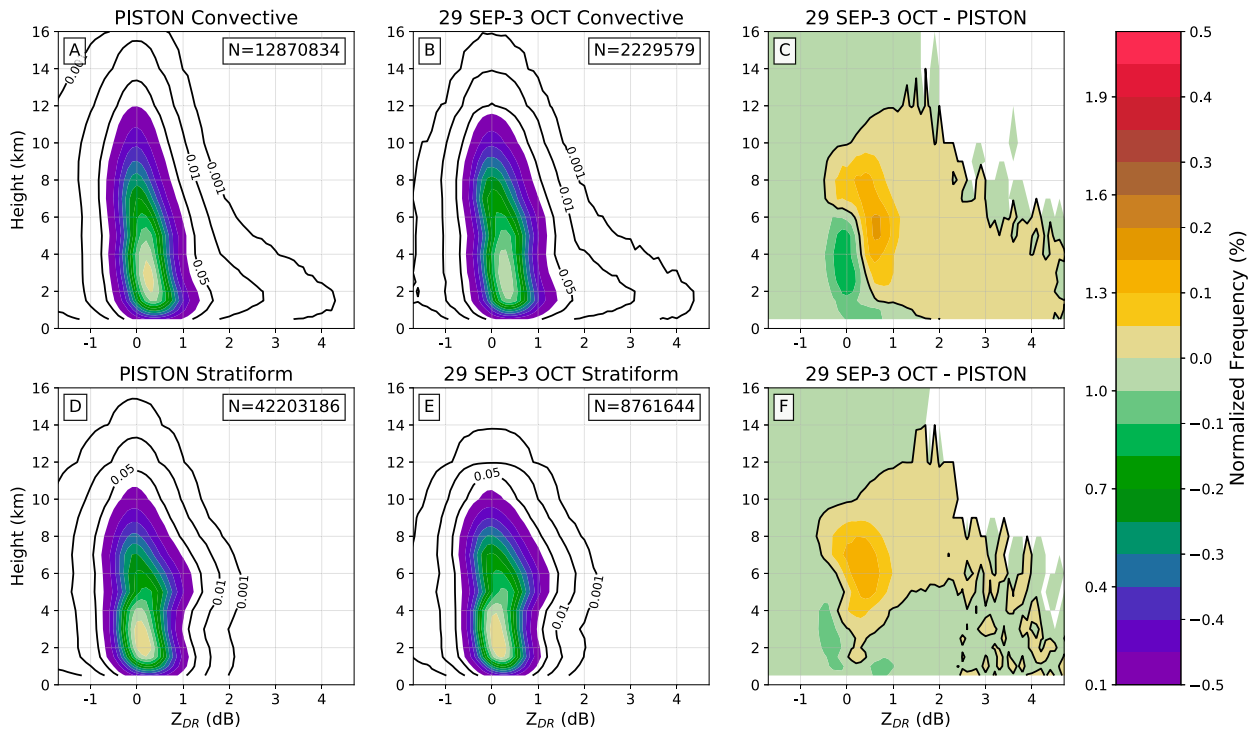


FIG. 4. As in Fig. 3, but for ZDR.

artificially enhancing the differences cannot be completely ruled out. While the cirrus canopy is present, convection at night tended to more frequently reach altitudes of 8–12 km. During the day, convection tended to be shallower with more intense reflectivity at low- to midlevel altitudes between 2 and 6 km. This day–night difference in convection suggests that shortwave radiative heating during the day likely contributes to stabilizing the upper levels and reducing the height of the convection. The day–night difference CFAD for stratiform precipitation is shown in Fig. 6 and highlights a prevalence for more reflectivity above the melting level with slightly lower reflectivity values at night during the time period of interest. In contrast, during the daytime there are larger reflectivity values near and just above the melting level and more frequent smaller reflectivity values below the melting level in the stratiform precipitation. Overall the day–night differences in the upper levels of the stratiform CFADS is not significantly different than the PISTON wide distribution suggesting a consistent effect of shortwave radiation on stratiform regions. The top-heavy differential daytime warming of the cloud canopy seems to promote daytime lifting in the stratiform region, but stabilization against deep convection, which has been utilized to explain long-lived daytime, top-heavy stratiform signatures (Ciesielski et al. 2018; Ruppert and Klocke 2019).

We next analyze the soundings launched every three hours to investigate the role that the thermodynamic environment may play in controlling the differences in the distribution of convective clouds. Figure 7 shows the evolution of the potential temperature and relative humidity (RH) anomalies from the PISTON mean during the passage of Kong-rey. An

estimate of cloud-base height from the HSRL and the derived tropopause height are provided for reference. On each day from 0600 to 1200 LST (2100–0300 UTC) there is a pronounced warming of the upper levels, which is mostly between 8 and 14 km associated with direct solar heating within the cloud layers. A persistent cold anomaly remains just above the warm anomaly and just below the tropopause, which is likely due to longwave cooling at the cloud top from the strong vertical gradient in optical depth and associated flux divergence. It should be noted that Rivoire et al. (2020) showed that cooler temperature near and above the tropopause is only partially explained by radiative cooling, concluding that other processes such as convectively generated gravity waves or a dynamic response to the vortex are playing a modest role. From 1500 LST 29 September to 1200 LST 1 October, there is a warm anomaly along the estimated tropopause height which indicates the presence of thin cirrus clouds which causes persistent longwave warming. During the time period of interest there is enhanced RH shown in Fig. 7b, which suggests a favorable environment for deep convection. A favorable environment for deep convection has been suggested to be important for outward propagating diurnal pulses in the outflow (Ditchek et al. 2019a; Knaff et al. 2019). The largest RH anomalies at the mid- to upper levels around 4–12 km on from 30 September to 1 October correspond to the time where the R/V *Thomas G. Thompson* was closest to the typhoon center. The positive RH anomalies suggests that water vapor may have contributed to the mid-upper level temperature anomalies through absorption of shortwave radiation. The water vapor absorption of solar radiation is not strong enough to account for a majority of

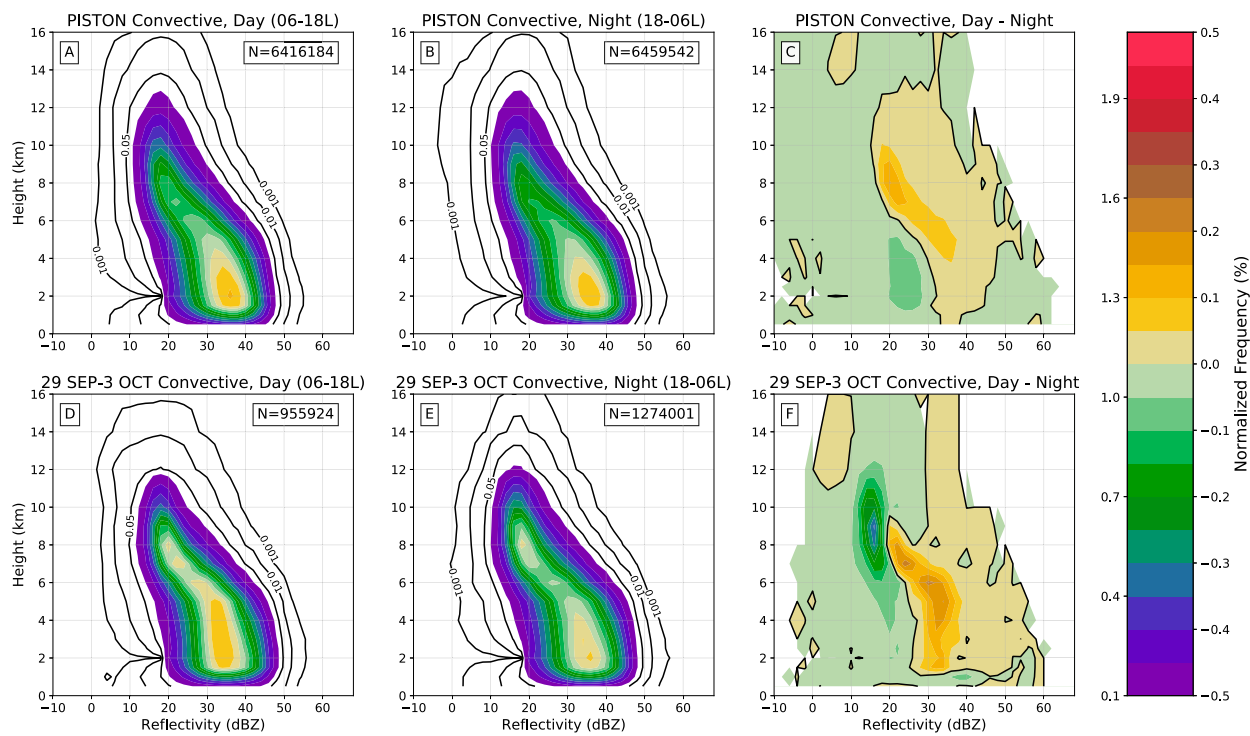


FIG. 5. CFADs separated into day (0600–1800 LST, 2100–0900 UTC) and night (1800–0600 LST, 0900–2100 UTC) for convectively defined points only, similar to Fig. 3. The PISTON CFAD during the (a) day, (b) night, and (c) the difference between them. The CFADs for the time of interest are shown during the (d) day, (e) at night, and (f) their difference. Observed convection is generally located in the outer core within ranges of 200–700 km.

the potential temperature anomalies though, which are due primarily to the shortwave absorption by hydrometeors.

The absorption of solar radiation by upper-level (8–15 km) clouds results in an increase in the potential temperature measured by the soundings. Increasing the vertical gradient in potential temperature stabilizes the upper-level cloud layer during the day, which can explain the reduction in height of the convective clouds observed in the CFADs in Figs. 5d–f. The strong TC outflow is primarily contained within the 2–3 km below the tropopause which suggests that the differences in reflectivity between 8 and 12 km can be largely attributed to radiative stabilization. In addition to stabilizing the upper levels, heating of the upper levels can affect the convective available potential energy (CAPE) of the environment. Figure 8 shows the distributions of CAPE, the convective inhibition (CIN), and the equilibrium level where parcels become neutrally buoyant. The CAPE and CIN are calculated by assuming irreversible pseudoadiabatic ascent of parcels with the mean thermodynamic conditions of the lowest 50 hPa of the atmosphere. Relative to the distributions during the entire PISTON campaign, there are no statistically significant differences in any of the variables during the time period of interest. The cumulative distribution function (CDF) of the normalized events suggests slightly larger CAPE values and lower CIN, but the equilibrium level was consistently on the low end of the pressure level. The distribution of CAPE is quite variable over the period, with on average lower CAPE values around

2070 J kg^{-1} during the day compared to an average of 2210 J kg^{-1} at night (Fig. 8d). Local increases in CAPE at night were also found in Tang and Zhang (2016). The largest values of CAPE were observed at night over each 24-h period up to 3000 J kg^{-1} . The variability due to radiation is smaller compared to that of the rapid consumption of CAPE by convection and subsequent regeneration. The nocturnal decline in CAPE due to consumption by convection is evident from 1800 LST 2 October to 0100 LST 3 October where there is a shift in the peak of the distribution of brightness temperatures from 245 to 215 K (Fig. 11a). The observations suggest that the overall thermodynamics of the environment were not drastically different with the presence of the cirrus canopy or upper-level cloud layers but the environment was favorable for deep convection.

To summarize, this section has documented a cirrus canopy extending over the ship for multiple days with a variety of observations being collected underneath the upper-level cloud layers. In the rainbands of Typhoon Kong-rey, the convective and stratiform cloud distributions were different compared to the total distributions during PISTON, with higher frequencies of ice phase clouds but overall shallower echo tops. The diurnal cycle of convection was more pronounced due to the strong shortwave absorption and stabilization of the clouds, which caused daytime convection to be shallower. It should be noted that in comparing the areal observations from SEA-POL and the semi-Lagrangian soundings, we make the assumption that the soundings provide

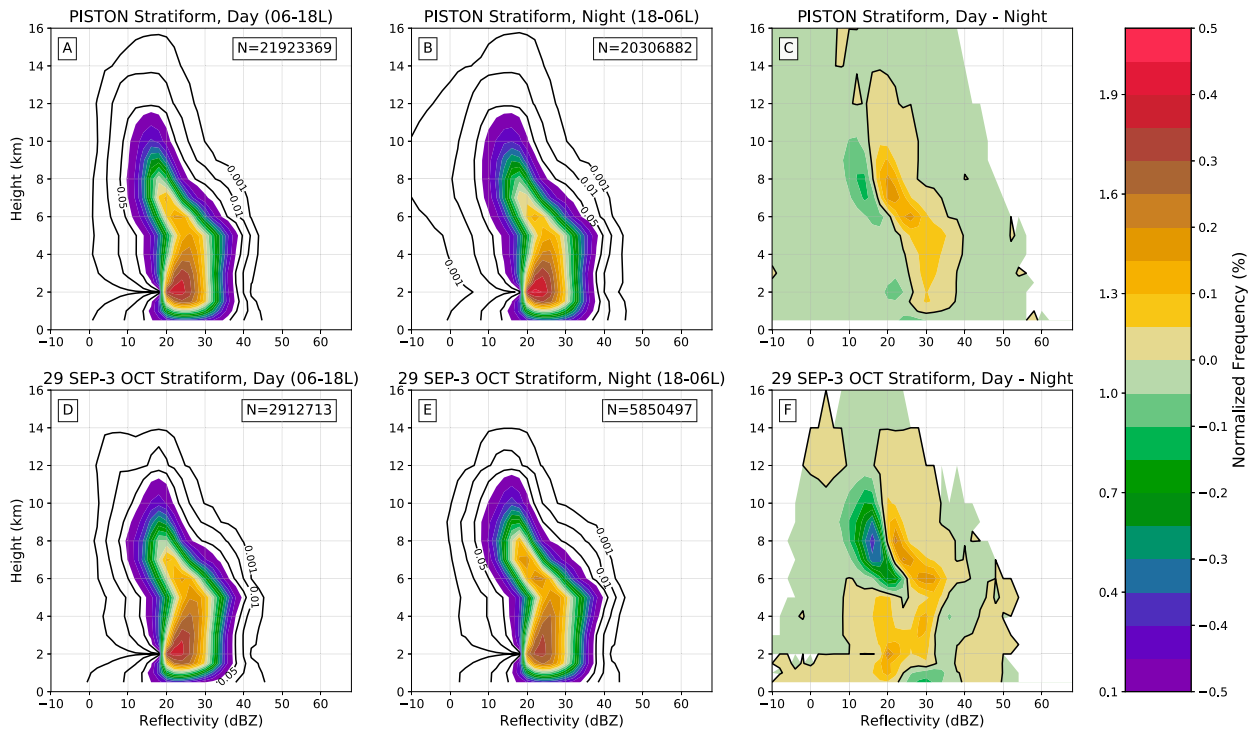


FIG. 6. As in Fig. 5, but for stratiform defined points.

a representative thermodynamic profile for the given area. The validity of this assumption is difficult to address because although the R/V *Thomas G. Thompson* is not moving, the center of Typhoon Kong-rey is continuously changing which causes the observations to vary in both storm relative quadrants and radii with time. The impact of the cirrus canopy and upper-level clouds on the vertical structure of convection during the diurnal cycle cannot be quantified directly in the observations or through radiative transfer as the altitude and thickness of the cirrus layer are unknown.

4. Diurnal pulses in the cirrus canopy

In the previous section we documented the evolution of convective and stratiform clouds under the cirrus canopy, including their diurnal variability. The area of the cirrus canopy itself has also been shown to have a diurnal cycle (Wu and Ruan 2016). Figure 9 shows the evolution of axisymmetric mean brightness temperatures from *Himawari-8* centered on Typhoon Kong-rey. The white and gray lines highlight the 208- and 240-K mean brightness temperature, which was shown to have a pronounced diurnal cycle in the blended IR imagery in Wu and Ruan (2016). In Fig. 9, the presence of cold clouds < 208 K is consistently found near the TC center, and as Kong-rey rapidly intensifies, the coldest clouds (< 208 K) shift radially outward with the eye becoming well established after 0900 LST 1 October. The radial extent of the cirrus canopy conversely contracts with time as Typhoon Kong-rey rapidly intensifies, in agreement with past studies showing the inverse relationship between areal extent of the cirrus canopy

and TC intensity (Browner et al. 1977; Kossin 2002). The areal extent of the cirrus canopy using the 240-K contour did not show a consistent diurnal cycle and did not exhibit the expected late afternoon maximum in contrast to previous studies (Steranka et al. 1977; Browner et al. 1977; Kossin 2002; Wu and Ruan 2016). Over the three days shown, there are three distinct times where regions of cold brightness temperatures propagate radially outwards from the TC center as evident by the 220-K shaded contour. The location of the R/V *Thomas G. Thompson* relative to the typhoon is shown to highlight that the observations collected from the ship sampled, at different storm relative radii, at most two outward propagating rings of cold IR temperatures.

In Fig. 9, the three distinct times where clouds colder than 220 K expand radially outward all occur roughly 24 h apart, which suggests that the diurnal cycle of radiation is important. The 220-K brightness temperature contour in the azimuthal mean best highlights the diurnal oscillations in the upper-level clouds but is an arbitrary value because of the tropical cyclone asymmetries. Dunion et al. (2014) found that outward propagating cold rings in the brightness temperatures are a consistent feature in mature TCs in the Atlantic and a climatology of Atlantic TCs by Ditchek et al. (2019a) further demonstrated the commonality of these diurnal pulses. The diurnal cycle of rainband convection therefore may be complicated by the tropical cyclone secondary circulation and the presence of diurnal pulses in the outflow layer (Dunion et al. 2014, 2019). To better isolate the diurnal oscillations in the brightness temperatures and to be consistent with the diurnal pulse literature, we examine the axisymmetric 6-h IR brightness

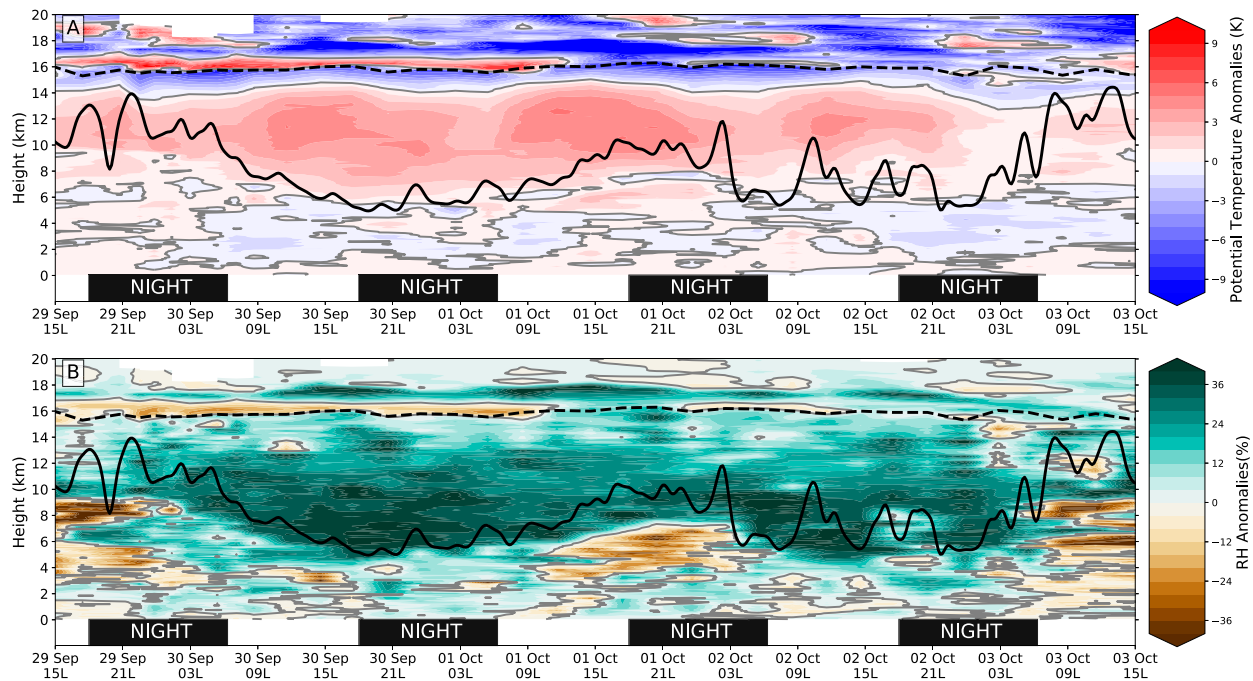


FIG. 7. (a) Potential temperature anomalies and (b) relative humidity anomalies from the PISTON mean profile. Missing data are white. The zero anomaly line is highlighted with the gray line. The black dashed line is the World Meteorological Organization (WMO) defined lapse rate defined tropopause (WMO 1957). The solid black line is a crude cloud-base estimate from the maximum backscatter of HSRL that has been filtered 10 times using a 1–2–1 filter. Night is denoted by the boxes within each subplot.

temperature differences in Fig. 10. Figure 10 includes black lines indicating the expected timing and position of diurnal pulses based on the “Dunion clock,” similar to those in Fig. 9. Figure 10 confirms that the diurnal oscillations in the axisymmetric brightness temperatures are diurnal pulses that propagate radially and form just outside the storm center. The three diurnal pulses are evident in the regions of colder temperatures (warmer colors), in addition to a coherent warming pulse that follows the first diurnal pulse. These three radially propagating cold rings that appear in Typhoon Kong-rey are not on the proposed Dunion clock since they occur ~6 h prior to the earliest expected time given in Dunion et al. (2014). The warming pulse occurs at the expected time of the cooling pulse on the Dunion clock, and similar long-lived warming pulses were found to occur in ~8.5% of the TC days analyzed in Ditchek et al. (2019a). The structure and timing of the warming pulse seems to be a response to the cooling pulse, such that the on-the-clock warming pulse found in previous studies may better highlight the presence of off-the-clock cooling pulses preceding them. The remainder of the study will focus on the observed cooling pulses.

Although the cooling pulses all occur on a diurnal cycle, the representation in the axisymmetric brightness temperatures and 6-h difference field are slightly different. The first and last diurnal pulses appear to start in the inner core of Typhoon Kong-rey around 1500–2100 LST and propagate outwards at colder brightness temperatures < 210 K, which slowly warms with time as the leading cloud edge subsides. The second pulse initiating on 30 September does not appear initially to be

coupled with the <210-K brightness temperatures in the inner core region but instead appears as a continuous outward expansion of cold clouds (Fig. 9). The 6-h difference evolution of the second diurnal pulse shows that cloud-top cooling did occur in the inner-core region near 100 km in the afternoon (~1500 LST) before propagating outward. To highlight the spatial differences in the first two diurnal pulses, Figs. 11a and 11b shows 6-h differences in the IR brightness temperatures centered on Typhoon Kong-rey on the two separate days corresponding to the red and blue horizontal lines in Fig. 2. It is important to note the difference in color scales between Figs. 11 and 10, because the amplitude of the axisymmetric diurnal pulses are reduced considerably due to the storm asymmetries caused by vertical wind shear and structural changes as Kong-rey rapidly intensified. The “cold rings” in Typhoon Kong-rey appear to be more asymmetric than those documented in previous studies, which is due to the presence of moderate northeasterly deep layer shear. The deep layer shear was low in all of the cases examined in Dunion et al. (2014) and is believed to be a requirement for robust diurnal oscillations (Knaff et al. 2019). In the climatology created by Ditchek et al. (2019a), long-lived cooling pulses were found less frequently in TCs with strong vertical wind shear, but only 6.8% of all long lived cooling pulses covered greater than 50% of radial rings suggesting that asymmetries may be more common than initially thought. Despite some differences in timing and structure of the cold rings in Typhoon Kong-rey compared to those previously reported, the overall appearance in satellite imagery is similar to past cases and suggests

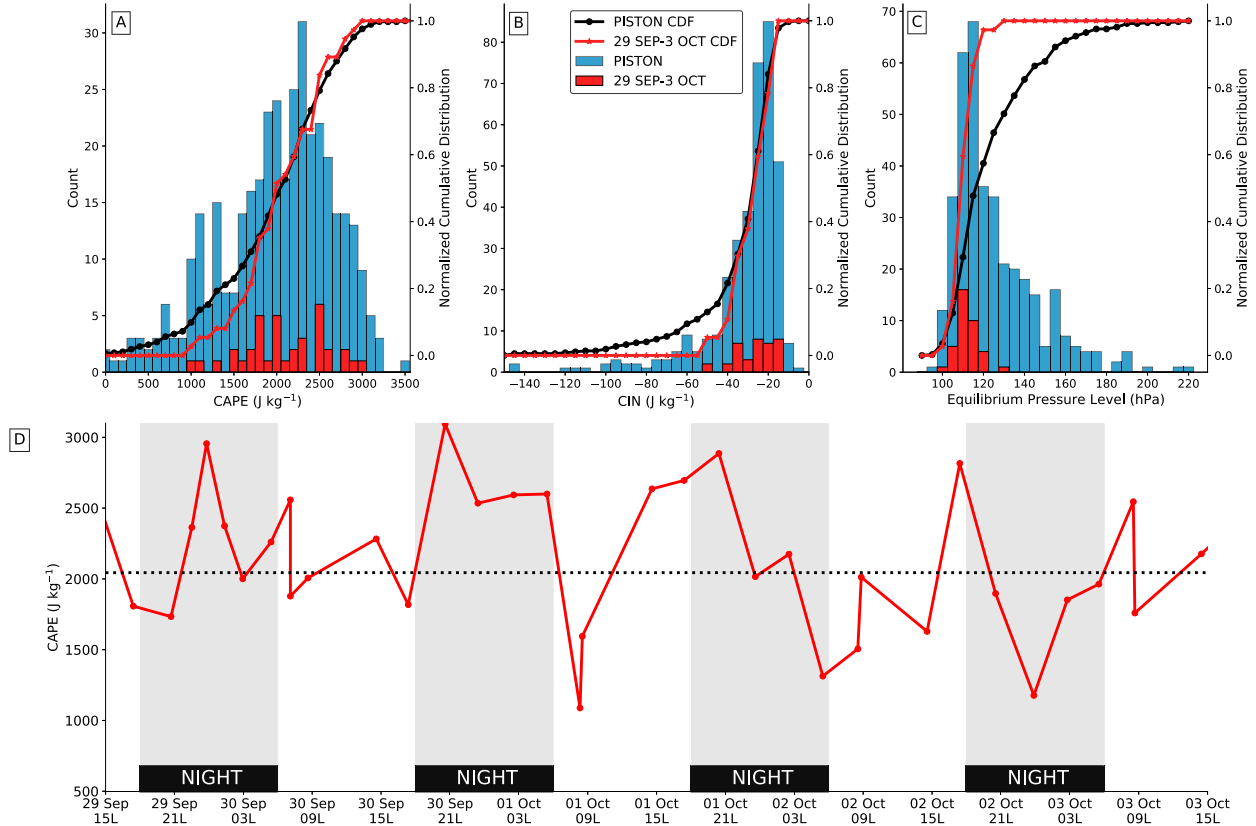


FIG. 8. The distributions of (a) convective available potential energy, (b) convective inhibition, and (c) equilibrium pressure level with bins of 100 J kg^{-1} , 5 J kg^{-1} , and 5 hPa , respectively. The distributions are shown for the entire PISTON field campaign (blue) and for the time period of interest during Typhoon Kong-rey (red). The black and red lines are the cumulative distribution functions (CDF) for each of the variables for the whole PISTON distribution and the distribution during the time frame of interest. (d) The temporal evolution of CAPE is shown with nighttime noted. The black dashed line is the mean CAPE from PISTON.

that the physical mechanisms that produce them may also be similar.

The three outward propagating rings of cold brightness temperature are evident in Fig. 10, but each vary in how far they propagate. The first diurnal pulse seems to propagate to the farthest radii while the third diurnal pulse only reaches to approximately 350 km. While the contraction of radial extent of the diurnal pulse contracts with Kong-rey's intensity, it is unclear if this contraction is related to or a function of the contraction of the cirrus canopy shown in previous studies (Browner et al. 1977; Kossin 2002). Despite the contraction of radial extent, the propagation speed of the diurnal pulses seems to increase with the intensity of the Typhoon Kong-rey. The propagation speed of the first pulse is qualitatively the slowest pulse, but all three are within the estimated propagation speed of those presented in Dunion et al. (2014). The propagation speeds range between 5 and 9 m s^{-1} , which is comparable to the $5\text{--}10 \text{ m s}^{-1}$ noted by Dunion et al. (2014) and the $8\text{--}14 \text{ m s}^{-1}$ shown in Ditchek et al. (2019a). The second diurnal pulse has a harder to define propagation speed because the cooling trend in Fig. 10 suggests that the diurnal pulse accelerated away from the inner core. The propagation speed of the second diurnal pulse from 400 to 500 km ($\sim 9 \text{ m s}^{-1}$) is

qualitatively faster than the propagation speeds from 200 to 300 km ($\sim 5 \text{ m s}^{-1}$). The different propagation speeds between the cooling pulses of Typhoon Kong-rey may be explained by the different intensities of the storm at the time. More intense tropical cyclones have a stronger secondary circulation that would support faster transport of ice away from the storm center in the outflow layer (Pendergrass and Willoughby 2009). The upper-level moisture could also play a role in modifying the pulses, although the environment shown in Fig. 7 did not show considerable variability from the ship's position over the time period of interest (Knaff et al. 2019).

It is uncertain how much of the brightness temperature signal of the cooling pulses is driven by ice being advected by inner core convection or ice produced by deep convective clouds in the outer core. Wu and Ruan (2016) discussed the possibility that diurnal pulses correspond to expansion and contraction of the cirrus canopy. If we focus only on the 220-K brightness temperature contour of Fig. 9, there are clear radial minima during the time of peak solar heating around local noon, which expands radially in the afternoon and into the overnight hours. The local minima further suggest that convective cloud heights observed by SEA-POL were reduced due to shortwave heating. The 208-K contour, which corresponds

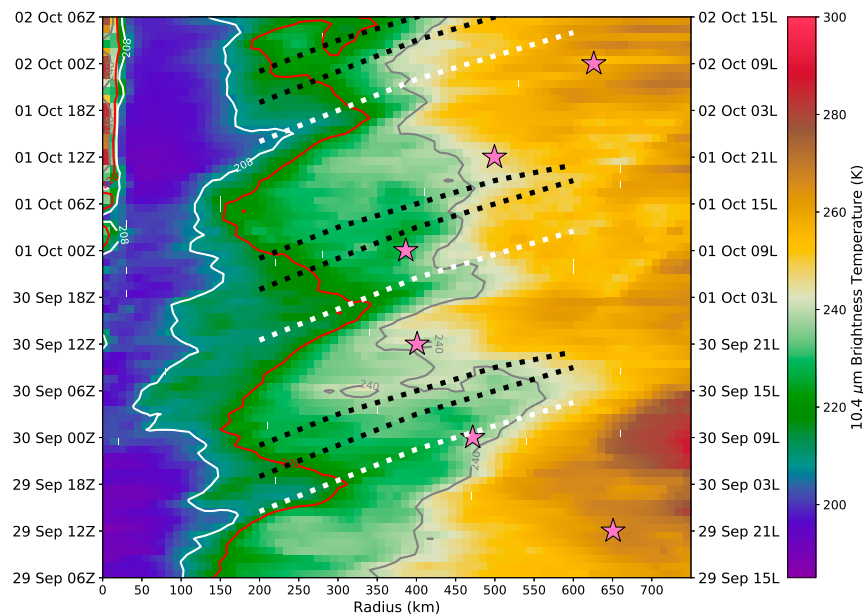


FIG. 9. Evolution of TC centered axisymmetric mean infrared brightness temperatures from *Himawari-8* averaged over 10-km bins every hour. Stars indicate the location of the R/V *Thomas G. Thompson* at 12-h intervals. The black dotted lines encapsulate the earliest and latest estimated times at the given radius of the cold clouds within the diurnal pulses from [Dunion et al. \(2014\)](#). The white dotted lines highlight the observed diurnal pulses. The thin white and gray lines are the 208- and 240-K brightness temperatures contours for comparison with [Wu and Ruan \(2016\)](#). The 220-K brightness temperature contour is shown in red. Data are shown hourly using linearly interpolated TC track data from JTWC. The right ordinate is in local time with the left ordinate being in UTC.

to deep convective clouds in [Wu and Ruan \(2016\)](#), does show a peak in area from 2100 to 0300 LST which corresponds to the outward propagating cold rings. This suggests that deep convection in the eyewall region of Typhoon Kong-rey is peaking in the late evening to early morning time period consistent with previous observations (e.g., [Gray and Jacobson 1977](#)). The 240-K contour, which could be used to identify the radial extent of cold clouds, expanded during the diurnal pulses but contracted to smaller radii with time as Kong-rey intensifies. The difference between the area of 208–240-K brightness temperature did not exhibit any strong diurnal variation.

To better understand the structure of these propagating diurnal pulses we utilize the observations underneath the cirrus canopy from the R/V *Thomas G. Thompson*. [Figure 12](#) shows the evolution of the median reflectivity profile every hour measured by SEA-POL with individual volume scans gridded at a height of 2 km shown at specific times. In addition, we plot the radial wind relative to the typhoon center exceeding 20 m s^{-1} derived from the soundings. There are two outward propagating cold rings observed from satellite that approach the location of the ship but at different storm relative distances. The edge of the first cooling pulse reaches the ship around 0500–0700 LST 30 September with the coldest clouds overhead being around 1200 LST 30 September ([Fig. 9](#)). During the time of the first pulse there was an increase in the outflow near 15 km that is associated with the outward propagating cold ring. Maxima in radial winds that are temporally coherent within

the outflow layer are referred to herein as outflow jets. It should be noted that the strong outflow from 1500 to 2100 LST 29 September can be attributed to the background easterlies and not from the circulation of Typhoon Kong-rey. Associated with the first diurnal pulse there is an increase in the height of precipitating clouds as rainbands moved into range of SEA-POL ([Figs. 12b–d](#)). Following the first pulse and associated outflow jet, there was a lull in the radial outflow and both a decrease in height and median reflectivity of the observed precipitating clouds. The decrease in convection was associated with an increase in stratiform precipitation as shown by the 2-km horizontal cross section at 1700 LST 30 September in [Fig. 12e](#). Although [Dunion et al. \(2019\)](#) showed that convection associated with diurnal pulses decreases in height as it moves radially outward, we cannot reliably evaluate the height changes with radius using SEA-POL.

The leading edge of the second propagating cold ring reaches the ship between 0100 and 0200 LST 1 October with the coldest cloud tops overhead the ship around 0400 LST 1 October ([Fig. 9](#)). Similar to the first pulse, [Fig. 12a](#) shows that there is another outflow jet measured by the soundings followed by an increase in the observed reflectivity echo tops. The heights of the measured reflectivity reach the level of strong radial outflow, which suggests that the convection is strong enough to penetrate the stable layer and likely contributes to the maintenance of the cold ring signature from satellites. There is also an increase in the median reflectivity values

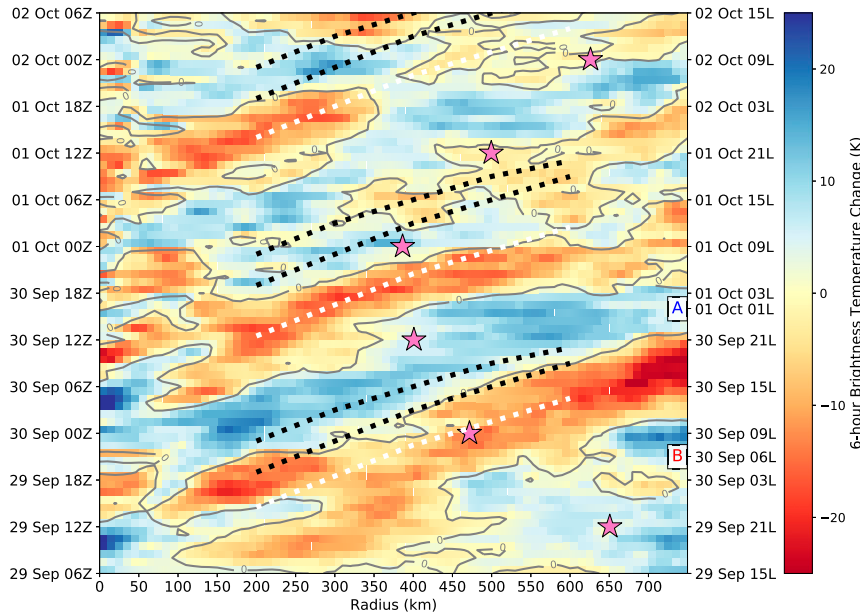


FIG. 10. Evolution of the TC centered axisymmetric mean 6-h difference infrared brightness temperatures from *Himawari-8* averaged over 10-km bins every hour. Stars indicate the location of the R/V *Thomas G. Thompson* at 12-h intervals. The black dotted lines encapsulate the earliest and latest estimated times at the given radius of the cold clouds within the diurnal pulses from Dunion et al. (2014). The white dotted lines highlight the observed diurnal pulse like features. The gray line indicates where there was zero difference between the 6-h difference imagery in the axisymmetric mean. The 6-h IR difference is shown hourly using linearly interpolated TC track data from JTWC. The right ordinate is in local time with the left ordinate being in UTC.

throughout the column corresponding to the times seen in the IR imagery with a small time lag. The median reflectivity at low levels increases after the elevated echo tops because of the moderate extent of stratiform precipitation in the SEA-POL domain (Fig. 12f). Following the increased outflow and rainband storm heights, there is a reduction of both the height and outflow magnitude in the hours following the second cooling pulse, which is similar to the previous cold ring and evident in the cross sections at 2 km at 0700 LST 1 October (Fig. 12g). After the second propagating cold ring there is a continuous period of median reflectivity values between 25 and 30 dBZ observed at lower levels due in part to a change in the ship heading and in the number of observed convective cells by SEA-POL.

Figure 12a shows that the outward propagating cold rings are coupled with an outflow jet and are followed by an increase in the height of precipitating clouds and an increase in the median reflectivity as convective squalls moved into range of SEA-POL. This suggests that the diurnal pulses observed here are convectively coupled. To further demonstrate the coupling, we show the evolution of the areal fraction of convective and stratiform classified points within the SEA-POL domain in Fig. 13a. Changes in ship motion, that have been subjectively defined, are labeled to explain discontinuities from one time to the next. The downward solar flux during PISTON is shown to help orient the reader to the solar cycle. The first diurnal pulse that moves over the ship around 0500–0700 LST 30 September

(2000–2200 UTC 29 September) corresponds to an increase in the observed areal extent of convection, lagged by several hours, which reaches a relative peak in coverage around 1400 LST 30 September. The amount of stratiform clouds also grew in areal extent following the pulses, suggesting a weakening of the convective band, which is consistent with IR satellite imagery. Trabing and Bell (2021) showed in an idealized model that there is an amplification of the heating/cooling profile of stratiform precipitation during the nighttime without strong shortwave radiation. The second pulse, which reached the ship between 0100 and 0200 LST 1 October, is followed by an increase in the areal extent of observed convection ~6 h later, similar to the first diurnal pulse. Around 8 h after the second pulse, SEA-POL observed fewer organized convective cells that were more scattered as Kong-rey moved away from the R/V *Thomas G. Thompson*. Following the second pulse between 1500 LST 1 October and 0300 LST 2 October is when dry air was observed in the soundings shown in Fig. 7b, which might help to explain the shallower echo tops and reduced convective area. Observations from SEA-POL support the idea that cold rings seen in IR imagery that propagate radially outwards are tied to convection but offset in time as radial winds in the outflow exceed the radial propagation speed of convective storms.

Fortunately, the second diurnal pulse was sampled multiple times by passive microwave sensors, allowing for a

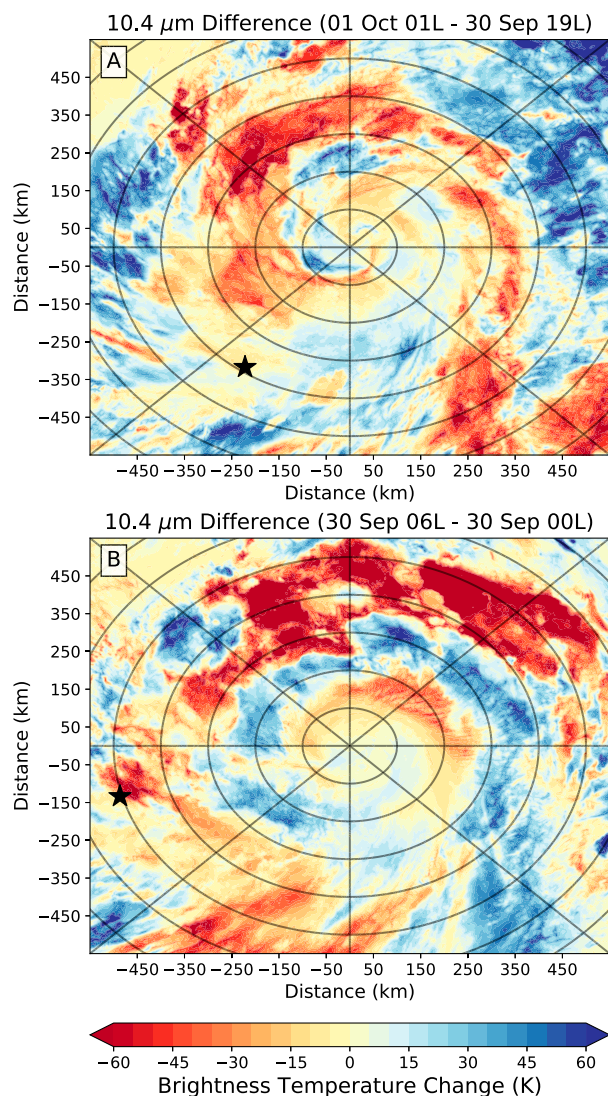


FIG. 11. Brightness temperature differences from the TC centered imagery of (a) 0100 LST 1 Oct minus 1900 LST 30 Sep and (b) the difference between 0600 LST 30 Sep and 0000 LST 30 Sep. The times of the 6-h IR brightness temperature differences are labeled in Figs. 2 and 10. Range rings are plotted every 100 km, and the black star is the mean location of the R/V *Thomas G. Thompson* over the 6 h.

complementary analysis to the infrared and radar observations. The first and third diurnal pulses did not have enough microwave passes for a complete analysis. Figure 14 shows five passes with good spatial coverage centered on Typhoon Kong-rey's position on 30 September in UTC time. The times shown are not evenly spaced and the satellites do not all have the same spatial resolution. On 1500 LST 30 September (Fig. 14a), there is a primary rainband wrapping into the center of the typhoon with a smaller area of deep convection at the center. The band is primarily located within 100 km of the storm center and has cold 91.6-GHz brightness temperatures, suggesting a large amount of scattering by ice and snow. By 1800 LST, the

primary rainband has widened and become more symmetric around the center, and has even colder brightness temperatures. At 1800 LST the primary rainband has moved radially outward and is now located just outside 100 km from the storm center. The next overpass by AMSR2 occurs 7 h later at 0100 LST 1 October, providing a more detailed look at Typhoon Kong-rey because of AMSR2's higher spatial resolution (Fig. 14c). Typhoon Kong-rey at 0100 LST has continued to intensify with convective ice signatures forming an eyewall within 100 km. The primary rainband has continued to move radially outward to >200 km away from the center. The structure of the rainband has become more disorganized at the next overpass at 0400 LST with discontinuous areas of deep convective ice signatures (Fig. 14d). The edge of the convective portion of the rainband has become harder to identify as it moves radially outwards to ~250 km. At this time, there also appears to be a new line of thunderstorms forming around 150 km away from the center as a new primary rainband begins to form. The last overpass by SSMIS shown at 0700 LST, shows that the radially outward propagating convective signature has been reduced in the azimuthal direction. After the convection associated with the primary rainband showed signs of weakening, it is unclear if there was a reorganization of the band or if it began to propagate azimuthally outside of the satellite's field of view. An estimate of the radial phase speed of the rainband from the microwave imagery is $\sim 3\text{--}8 \text{ m s}^{-1}$ which is similar to what was observed from the IR imagery. The collocation of the microwave imagery with the infrared imagery suggests that the outward propagating cold rings were convectively coupled and originated from the primary rainband, which moved radially outwards.

This section has shown that within the cirrus canopy of Typhoon Kong-rey there were multiple outward propagating cold rings occurring on a diurnal timeline. Multiple perspectives were analyzed using satellites and ship based instruments to provide an in depth look at the cold rings. The cooling pulses were evident in the IR imagery as an expansion and contraction of the cold IR clouds, but were manifested in the typhoon dynamics as an outflow jet observed by upper-air soundings. Associated with the cold IR clouds, there was an increase in convection observed from the R/V *Thomas G. Thompson* with a lag time of roughly six hours suggesting that these features are in fact convectively coupled. Convective heights sometimes penetrated the outflow layer suggesting that rainbands may continually contribute to the diurnal pulse signatures in the IR. Although these cold rings did not occur at the typical times proposed by Dunion et al. (2014), the characterizing features are similar to what was proposed in the modeling study of Dunion et al. (2019). Whether these diurnal pulses are the same phenomena just modulated by Kong-rey's asymmetric structure and environment with moderate vertical wind shear, or if they are representative of a different physical mechanism is unclear from the limited observations available.

5. Summary and conclusions

In this study we have used novel observations from the Propagation of Intraseasonal Tropical Oscillations (PISTON) field campaign to explore the diurnal variability of convection

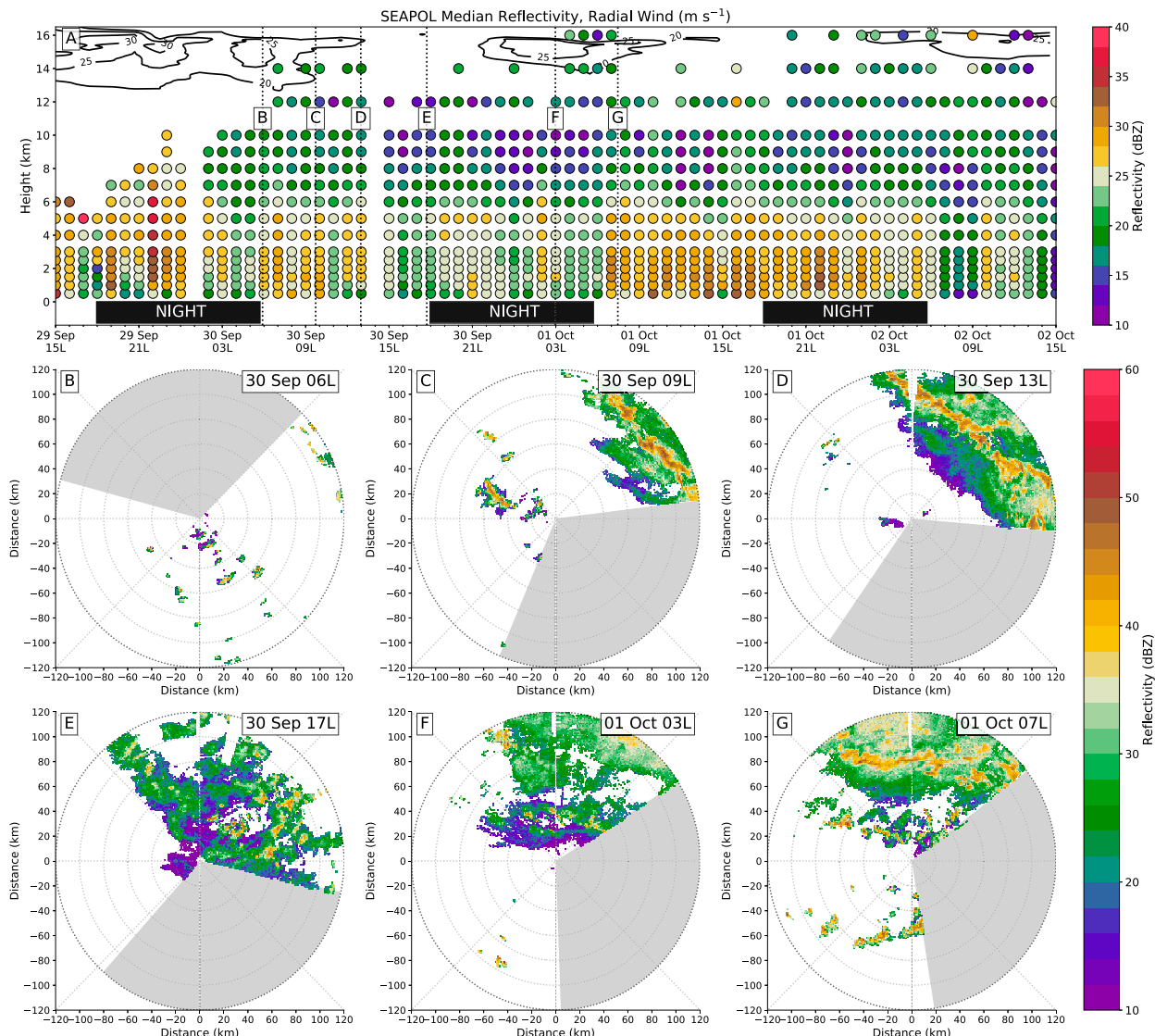


FIG. 12. Colored circles in (a) are the evolution of the hourly median reflectivity profile from gridded SEA-POL data. Contoured in black are the tropical cyclone relative radial winds derived from the thermodynamic profiles exceeding 20 m s^{-1} . (b)–(h) Vertical dotted lines indicate the times of the corresponding 2-km altitude horizontal cross sections. The gray shaded region is where SEA-POL was not transmitting and collecting observations, which changes with ship heading. Times where no solar radiation is affecting the cloud distributions are denoted for reference. Both color bars use increments of 2 dBZ ; however, the evolution of the median reflectivity and the cross sections use slightly different color bars because of the differences in the range of values.

under a distribution of cold upper-level clouds. Observations over a three day span were collected under the cirrus canopy of Super Typhoon Kong-rey (2018) and compared to the two months of observations from PISTON. Satellite observations show evidence of diurnal oscillations in the brightness temperature of upper-level clouds. The case study of Typhoon Kong-rey has provided unique observations of the diurnal variability of rainband convection and diurnal oscillations in the outflow layer for future comparison with and improvement of numerical weather prediction models.

Observations from PISTON provide evidence that the convective and stratiform clouds under the cirrus canopy of

Typhoon Kong-rey were stronger compared to the overall distribution from PISTON. The peak altitude of convective and stratiform clouds, however, was reduced in the near TC environment and believed to be due to the increased stability from the outflow layer (Houze 2010). The elevated moisture in the environment of Typhoon Kong-rey may be responsible for the increased median size of snow and ice found at upper levels in both convective and stratiform precipitating clouds. On diurnal time scales, a temperature response to shortwave heating was observed in the thermodynamic soundings and in rainband convection with reduced concentrations of ice aloft. These observations suggest that the stabilizing effect

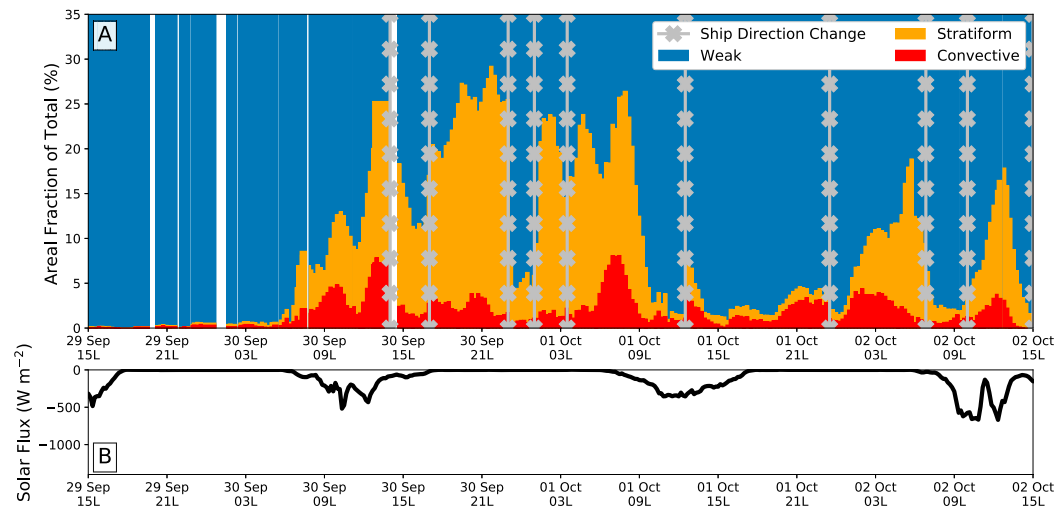


FIG. 13. (a) Temporal evolution of the areal coverage of convective and stratiform precipitation during the time period of interest observed by SEA-POL. Gray vertical lines with bold “x” indicate substantial turns in the motion of the R/V *Thomas G. Thompson* where previously observed radar echoes were obscured in the following radar scan. The white region is where no data were collected. (b) The measured solar flux is shown, which is negative to denote that the fluxes are downward.

of shortwave radiation in the moat region and in upper levels of the rainbands shown in the modeling studies of Tang et al. (2017) and Trabing and Bell (2021) may be at work; however, the shortwave radiation also led to stronger ice signatures aloft in stratiform regions consistent with Ciesielski et al. (2018) and Ruppert and Klocke (2019). We cannot evaluate the Gray and Jacobson (1977) mechanism for explaining the diurnal cycle of oceanic convection due to the continuous changes in boundary layer winds associated with nearby convective rainbands and the increasing radial winds during Kong-rey’s intensification.

Observations of Typhoon Kong-rey have revealed diurnal oscillations in the brightness temperature that have characteristics similar to previously reported diurnal pulses (Dunion et al. 2019; Ditchek et al. 2019a; Knaff et al. 2019). The cooling pulses in Typhoon Kong-rey were not on the “Dunion clock,” similar to the cooling pulse noted by Ditchek et al. (2020), but three such oscillations occurred in the outflow of Typhoon Kong-rey suggesting that the feature is diurnally driven and recurrent. A warming pulse on the Dunion clock was also found following the first diurnal pulse, suggesting that on-the-clock warming pulses may be an indicator of off-the-clock cooling pulses. The R/V *Thomas G. Thompson* was in range to observe the convective evolution of rainbands associated with two of the diurnal pulses found in Typhoon Kong-rey during its rapid intensification. The cooling pulses were associated with maxima in the outflow (outflow jets), consistent with the model shown in Dunion et al. (2019) and the model analysis in Ditchek et al. (2020). The increasing convection after the cooling pulse in the outflow and in the IR imagery suggests a lagged coupling with rainband convection. Observations from SEA-POL and the thermodynamic soundings showed convective reflectivity echoes penetrating the outflow layer suggesting that the cooling pulses at upper levels are coupled with, and likely maintained by, rainband convection and are not

driven solely by inner-core convective processes of Typhoon Kong-rey. The maintenance of the cooling pulses by strong rainband convection is further suggested by the favorable environment for deep convection shown by previous studies (Dunion et al. 2019; Knaff et al. 2019; Ditchek et al. 2019a).

One proposed mechanism for the cooling pulses in mature TCs is through the excitation and coupling of gravity waves to convection in the outer core (O’Neill et al. 2017; Evans and Nolan 2019; Dunion et al. 2019; Ditchek et al. 2019a). Gravity waves have been tied to the diurnal cycle of convection, which has been shown to peak in the early morning; however, if this peak in convection was modified through asymmetric tropical cyclone dynamics caused by the moderate vertical wind shear or the presence of a cirrus canopy, the timing of cooling pulses could also be modified (Hong et al. 2006). This indicates that outward propagating cold rings may not be diurnally locked, but can vary in different environments. It is unclear exactly why the propagating cold rings in the brightness temperatures of Typhoon Kong-rey did not occur on the Dunion clock, although the diurnal cycle of convection in oceanic tropical environments can be variable. Variations in diurnal TC convective activity have been shown to have basin differences, for example lightning associated with deep convection in the TC inner core showed a broader diurnal peak in the east Pacific (2300–0800 LST) compared to the Atlantic (2300–0200 LST) (Stevenson et al. 2016). We therefore speculate that similar, if not the same, mechanisms are controlling the diurnal oscillations seen in Kong-rey to those seen in the Atlantic, but further research is required to confirm this hypothesis. It should also be emphasized that this study has an inherently limited sample size, and as such some differences can be attributed to the stochastic development of rainband convection.

The diurnal oscillations in the brightness temperature imagery of Typhoon Kong-rey occurred while the tropical cyclone was

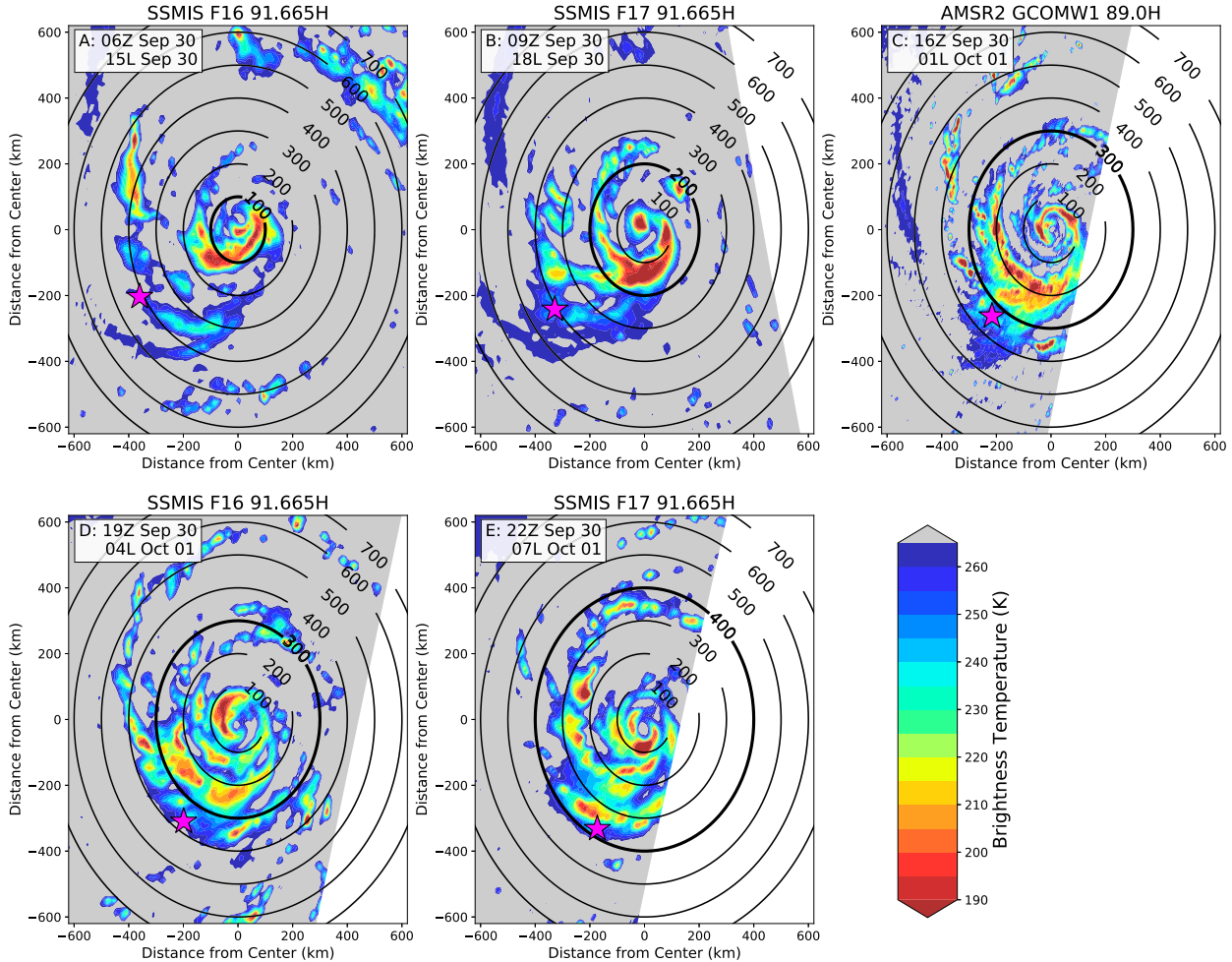


FIG. 14. Sequence of passive microwave overpasses during the second diurnal pulse from SSMIS and AMSR2 centered over Typhoon Kong-rey. The UTC times shown are all on 30 Sep at (a) 0600, (b) 0900, (c) 1600, (d) 1900, and (e) 2200 UTC. The corresponding local solar time is also denoted. The SSMIS imagery shown corresponds to the 91.655-GHz band while the AMSR2 imagery is from the 89.0-GHz band. Brightness temperatures warmer than 265 K are gray, and locations outside of the field of view are white. The pink stars indicate the general location of the R/V *Thomas G. Thompson* during the time of the overpass. Range rings are plotted every 100 km extending out to 700 km. The bold range ring indicates the approximate radius of the cold IR brightness temperatures from Fig. 9.

rapidly intensifying suggesting that these oscillations can occur at all stages of development consistent with past studies (Knaff et al. 2019; Ditchek et al. 2019a). The upper-level oscillations show variability in propagation speed which could be directly tied to the strength of the secondary circulation. The microwave imagery suggests that the convective evolution of these rings can be asymmetric, aligning with the vertical wind shear vector, which when azimuthally averaged could explain variations in the intensity of cooling pulses. A radial contraction of the secondary circulation with increased subsidence closer to the center, could also lead to changes in the propagation and magnitude of IR temperatures which has been thought to explain the inverse relationship between cirrus canopy extent and tropical cyclone intensity (Browner et al. 1977). Understanding the variability of these diurnal oscillations both spatially and temporally due to factors such as vertical wind shear and storm motion will be necessary to

improve short term quantitative precipitation forecasts and will be a topic for future work.

The observations analyzed herein were collected in a continuously evolving environment and have some observational biases from the position of the R/V *Thomas G. Thompson*. Relative to Typhoon Kong-rey, the observations were collected at different storm relative locations, which is important for considering diurnal pulses, which are expected at different storm relative radii at specific times. The changing storm relative position is one complication to the study as it is evident that the physical processes affecting the diurnal cycle varies between the regions of the TC. Despite some expected slight inconsistencies between the different instrumentation and limited areal coverage from SEA-POL, the Lagrangian balloon-borne thermodynamic profiles, and the ship-based fluxes, the collected data provide a coherent narrative. These are the first known surface-based oceanic observations of diurnal oscillations in

the upper-level clouds of a tropical cyclone, providing further evidence that radiation affects the distribution of convective and stratiform clouds in the rainbands during intensification. Further case studies and observations are warranted to improve and expand upon the results of this study.

Acknowledgments. This work has been funded by the Office of Naval Research Award N000141613033. The authors thank Chelsea Nam and Jennifer DeHart for their insightful comments. This work has also been improved by the comments of three anonymous reviewers. Meteorology and surface flux data collected during PISTON are available at the NOAA Physical Sciences Laboratory (PSL) ftp site: ftp://ftp1.esrl.noaa.gov/psd3/cruises/PISTON_MISOBOB_2018/TGT/. Multiple datasets from PISTON, such as the radiosondes and SEA-POL gridded data, are available from <https://www-air.larc.nasa.gov/cgi-bin/ArcView/camp2ex>.

REFERENCES

- Bell, M. M., M. Dixon, B. Javornik, W.-C. Lee, B. Melli, J. DeHart, and T.-Y. Cha, 2019: nsf-irose/irose-blaze: Irose-blaze-20190105. Zenodo, accessed 9 April 2019, <https://doi.org/10.5281/ZENODO.2532758>.
- Bellenger, H., Y. N. Takayabu, T. Ushiyuma, and K. Yoneyama, 2010: Role of diurnal warm layers in the diurnal cycle of convection over the tropical Indian Ocean during MISMO. *Mon. Wea. Rev.*, **138**, 2426–2433, <https://doi.org/10.1175/2010MWR3249.1>.
- Bowman, K. P., and M. D. Fowler, 2015: The diurnal cycle of precipitation in tropical cyclones. *J. Climate*, **28**, 5325–5334, <https://doi.org/10.1175/JCLI-D-14-00804.1>.
- Browner, S. P., W. L. Woodley, and C. G. Griffith, 1977: Diurnal oscillation of the area of cloudiness associated with tropical storms. *Mon. Wea. Rev.*, **105**, 856–864, [https://doi.org/10.1175/1520-0493\(1977\)105<0856:DOOTAO>2.0.CO;2](https://doi.org/10.1175/1520-0493(1977)105<0856:DOOTAO>2.0.CO;2).
- Bu, Y. P., R. G. Fovell, and K. L. Corbosiero, 2014: Influence of cloud-radiative forcing on tropical cyclone structure. *J. Atmos. Sci.*, **71**, 1644–1662, <https://doi.org/10.1175/JAS-D-13-0265.1>.
- Ciesielski, P. E., P. H. Haertel, R. H. Johnson, J. Wang, and S. Loehrer, 2012: Developing high-quality field program sounding datasets. *Bull. Amer. Meteor. Soc.*, **93**, 325–336, <https://doi.org/10.1175/BAMS-D-11-00091.1>.
- , R. H. Johnson, W. H. Schubert, and J. H. Ruppert, 2018: Diurnal cycle of the ITCZ in DYNAMO. *J. Climate*, **31**, 4543–4562, <https://doi.org/10.1175/JCLI-D-17-0670.1>.
- Craig, G., 1996: Numerical experiments on radiation and tropical cyclones. *Quart. J. Roy. Meteor. Soc.*, **122**, 415–422, <https://doi.org/10.1002/qj.49712253006>.
- Ditchev, S. D., J. Molinari, K. L. Corbosiero, and R. G. Fovell, 2019a: An objective climatology of tropical cyclone diurnal pulses in the Atlantic basin. *Mon. Wea. Rev.*, **147**, 591–605, <https://doi.org/10.1175/MWR-D-18-0368.1>.
- , K. L. Corbosiero, R. G. Fovell, and J. Molinari, 2019b: Electrically active tropical cyclone diurnal pulses in the Atlantic basin. *Mon. Wea. Rev.*, **147**, 3595–3607, <https://doi.org/10.1175/MWR-D-19-0129.1>.
- , —, —, and —, 2020: Electrically active diurnal pulses in Hurricane Harvey (2017). *Mon. Wea. Rev.*, **148**, 2283–2305, <https://doi.org/10.1175/MWR-D-20-0022.1>.
- Dunion, J. P., C. D. Thorncroft, and C. S. Velden, 2014: The tropical cyclone diurnal cycle of mature hurricanes. *Mon. Wea. Rev.*, **142**, 3900–3919, <https://doi.org/10.1175/MWR-D-13-00191.1>.
- , —, and D. S. Nolan, 2019: Tropical cyclone diurnal cycle signals in a hurricane nature run. *Mon. Wea. Rev.*, **147**, 363–388, <https://doi.org/10.1175/MWR-D-18-0130.1>.
- Duran, P., and J. Molinari, 2016: Upper-tropospheric low Richardson number in tropical cyclones: Sensitivity to cyclone intensity and the diurnal cycle. *J. Atmos. Sci.*, **73**, 545–554, <https://doi.org/10.1175/JAS-D-15-0118.1>.
- , —, and —, 2019: Tropopause evolution in a rapidly intensifying tropical cyclone: A static stability budget analysis in an idealized axisymmetric framework. *J. Atmos. Sci.*, **76**, 209–229, <https://doi.org/10.1175/JAS-D-18-0097.1>.
- Evans, R. C., and D. S. Nolan, 2019: Balanced and radiating wave responses to diurnal heating in tropical cyclone-like vortices using a linear nonhydrostatic model. *J. Atmos. Sci.*, **76**, 2575–2597, <https://doi.org/10.1175/JAS-D-18-0361.1>.
- Fovell, R. G., K. L. Corbosiero, A. Seifert, and K.-N. Liou, 2010: Impact of cloud-radiative processes on hurricane track. *Geophys. Res. Lett.*, **37**, L07808, <https://doi.org/10.1029/2010GL042691>.
- , K. L. Bu, Y. P. Corbosiero, W. Tung, Y. Cao, H. Kuo, L. Hsu, and H. Su, 2016: Influence of cloud microphysics and radiation on tropical cyclone structure and motion. *Multiscale Convection-Coupled Systems in the Tropics: A Tribute to Dr. Michio Yanai, Meteor. Monogr.*, No. 56, 11.1–11.27, <https://doi.org/10.1175/AMSMONOGRAPHS-D-15-0006.1>.
- Gray, W. M., and R. W. Jacobson Jr., 1977: Diurnal variation of deep cumulus convection. *Mon. Wea. Rev.*, **105**, 1171–1188, [https://doi.org/10.1175/1520-0493\(1977\)105<1171:DVCODCC>2.0.CO;2](https://doi.org/10.1175/1520-0493(1977)105<1171:DVCODCC>2.0.CO;2).
- Hobgood, J. S., 1986: A possible mechanism for the diurnal oscillations of tropical cyclones. *J. Atmos. Sci.*, **43**, 2901–2922, [https://doi.org/10.1175/1520-0469\(1986\)043<2901:APMFTD>2.0.CO;2](https://doi.org/10.1175/1520-0469(1986)043<2901:APMFTD>2.0.CO;2).
- Hong, G., G. Heygster, and C. A. M. Rodriguez, 2006: Effect of cirrus clouds on the diurnal cycle of tropical deep convective clouds. *J. Geophys. Res.*, **111**, D06209, <https://doi.org/10.1029/2005JD006209>.
- Houze, R. A., Jr., 2010: Clouds in tropical cyclones. *Mon. Wea. Rev.*, **138**, 293–344, <https://doi.org/10.1175/2009MWR2989.1>.
- , S. A. Rutledge, T. J. Matejka, and P. V. Hobbs, 1981: The mesoscale and microscale structure and organization of clouds and precipitation in midlatitude cyclones. III: Air motions and precipitation growth in a warm-frontal rainband. *J. Atmos. Sci.*, **38**, 639–649, [https://doi.org/10.1175/1520-0469\(1981\)038<0639:TMAMSA>2.0.CO;2](https://doi.org/10.1175/1520-0469(1981)038<0639:TMAMSA>2.0.CO;2).
- Hughes, K. G., J. N. Moum, and E. L. Shroyer, 2020: Evolution of the velocity structure in the diurnal warm layer. *J. Phys. Oceanogr.*, **50**, 615–631, <https://doi.org/10.1175/JPO-D-19-0207.1>.
- Knaff, J. A., C. J. Slocum, and K. D. Musgrave, 2019: Quantification and exploration of diurnal oscillations in tropical cyclones. *Mon. Wea. Rev.*, **147**, 2105–2121, <https://doi.org/10.1175/MWR-D-18-0379.1>.
- Kossin, J. P., 2002: Daily hurricane variability inferred from GOES infrared imagery. *Mon. Wea. Rev.*, **130**, 2260–2270, [https://doi.org/10.1175/1520-0493\(2002\)130<2260:DHVIFG>2.0.CO;2](https://doi.org/10.1175/1520-0493(2002)130<2260:DHVIFG>2.0.CO;2).
- , and M. DeMaria, 2016: Reducing operational hurricane intensity forecast errors during eyewall replacement cycles. *Wea. Forecasting*, **31**, 601–608, <https://doi.org/10.1175/WAF-D-15-0123.1>.
- Leppert, K. D., and D. J. Cecil, 2016: Tropical cyclone diurnal cycle as observed by TRMM. *Mon. Wea. Rev.*, **144**, 2793–2808, <https://doi.org/10.1175/MWR-D-15-0358.1>.

- Li, Q., and Y. Wang, 2012: Formation and quasi-periodic behavior of outer spiral rainbands in a numerically simulated tropical cyclone. *J. Atmos. Sci.*, **69**, 997–1020, <https://doi.org/10.1175/2011JAS3690.1>.
- Mecikalski, J. R., and G. J. Tripoli, 1998: Inertial available kinetic energy and the dynamics of tropical plume formation. *Mon. Wea. Rev.*, **126**, 2200–2216, [https://doi.org/10.1175/1520-0493\(1998\)126<2200:IAKEAT>2.0.CO;2](https://doi.org/10.1175/1520-0493(1998)126<2200:IAKEAT>2.0.CO;2).
- Melhauser, C., and F. Zhang, 2014: Diurnal radiation cycle impact on the pregenesis environment of Hurricane Karl (2010). *J. Atmos. Sci.*, **71**, 1241–1259, <https://doi.org/10.1175/JAS-D-13-0116.1>.
- Merritt, E., and R. Wexler, 1967: Cirrus canopies in tropical storms. *Mon. Wea. Rev.*, **95**, 111–120, [https://doi.org/10.1175/1520-0493\(1967\)095<0111:CCITS>2.3.CO;2](https://doi.org/10.1175/1520-0493(1967)095<0111:CCITS>2.3.CO;2).
- Muramatsu, T., 1983: Diurnal-variations of satellite-measured TBB areal distribution and eye diameter of mature typhoons. *J. Meteor. Soc. Japan*, **61**, 77–90, https://doi.org/10.2151/jmsj1965.61.1_77.
- Navarro, E. L., and G. J. Hakim, 2016: Idealized numerical modeling of the diurnal cycle of tropical cyclones. *J. Atmos. Sci.*, **73**, 4189–4201, <https://doi.org/10.1175/JAS-D-15-0349.1>.
- , —, and H. E. Willoughby, 2017: Balanced response of an axisymmetric tropical cyclone to periodic diurnal heating. *J. Atmos. Sci.*, **74**, 3325–3337, <https://doi.org/10.1175/JAS-D-16-0279.1>.
- Nicholls, M. E., 2015: An investigation of how radiation may cause accelerated rates of tropical cyclogenesis and diurnal cycles of convective activity. *Atmos. Chem. Phys.*, **15**, 9003–9029, <https://doi.org/10.5194/acp-15-9003-2015>.
- O'Neill, M. E., D. Perez-Betancourt, and A. A. Wing, 2017: Accessible environments for diurnal-period waves in simulated tropical cyclones. *J. Atmos. Sci.*, **74**, 2489–2502, <https://doi.org/10.1175/JAS-D-16-0294.1>.
- Pendergrass, A. G., and H. E. Willoughby, 2009: Diabatically induced secondary flows in tropical cyclones. Part I: Quasi-steady forcing. *Mon. Wea. Rev.*, **137**, 805–821, <https://doi.org/10.1175/2008MWR2657.1>.
- Powell, S. W., R. A. Houze Jr., and S. R. Brodzik, 2016: Rainfall-type categorization of radar echoes using polar coordinate reflectivity data. *J. Atmos. Oceanic Technol.*, **33**, 523–538, <https://doi.org/10.1175/JTECH-D-15-0135.1>.
- Razin, N., P. J. Brown, C. J. Slocum, J. Knaff, M. M. Bell, 2021: Tropical Cyclone Precipitation, Infrared, Microwave, and Environmental Dataset (TC PRIMED). 34th Conf. on Hurricanes and Tropical Meteorology, 68, Amer. Meteor. Soc., <https://ams.confex.com/ams/34HURR/meetingapp.cgi/Paper/373164>.
- Rios-Berrios, R., 2020: Impacts of radiation and cold pools on the intensity and vortex tilt of weak tropical cyclones interacting with vertical wind shear. *J. Atmos. Sci.*, **77**, 669–689, <https://doi.org/10.1175/JAS-D-19-0159.1>.
- Rivoire, L., T. Birner, J. A. Knaff, and N. Tourville, 2020: Quantifying the radiative impact of clouds on tropopause layer cooling in tropical cyclones. *J. Climate*, **33**, 6361–6376, <https://doi.org/10.1175/JCLI-D-19-0813.1>.
- Rowe, A. K., R. A. Houze Jr., S. Brodzik, and M. D. Zuluaga, 2019: The diurnal and microphysical characteristics of MJO rain events during DYNAMO. *J. Atmos. Sci.*, **76**, 1975–1988, <https://doi.org/10.1175/JAS-D-18-0316.1>.
- Ruppert, J. H., and D. Klocke, 2019: The two diurnal modes of tropical upward motion. *Geophys. Res. Lett.*, **46**, 2911–2921, <https://doi.org/10.1029/2018GL081806>.
- , and M. E. O'Neill, 2019: Diurnal cloud and circulation changes in simulated tropical cyclones. *Geophys. Res. Lett.*, **46**, 502–511, <https://doi.org/10.1029/2018GL081302>.
- , A. A. Wing, X. Tang, and E. L. Duran, 2020: The critical role of cloud-infrared radiation feedback in tropical cyclone development. *Proc. Natl. Acad. Sci. USA*, **117**, 27884–27892, <https://doi.org/10.1073/pnas.2013584117>.
- Rutledge, S. A., V. Chandrasekar, B. Fuchs, J. George, F. Junyent, B. Dolan, P. C. Kennedy, and K. Drushka, 2019: SEA-POL goes to sea. *Bull. Amer. Meteor. Soc.*, **100**, 2285–2301, <https://doi.org/10.1175/BAMS-D-18-0233.1>.
- Schott, T., and Coauthors, 2012: The Saffir-Simpson hurricane wind scale. NOAA/National Hurricane Center, 4 pp., <https://www.nhc.noaa.gov/pdf/shsws.pdf>.
- Smith, W. P., M. E. Nichols, and R. A. Pielke, 2020: The role of radiation in accelerating tropical cyclogenesis in idealized simulations. *J. Atmos. Sci.*, **77**, 1261–1277, <https://doi.org/10.1175/JAS-D-19-0044.1>.
- Sobel, A. H., J. Sprintall, E. D. Maloney, Z. K. Martin, S. Wang, S. P. de Szoeke, B. C. Trabing, and S. A. Rutledge, 2021: Large-scale state and evolution of the atmosphere and ocean during PISTON 2018. *J. Climate*, **34**, 5017–5035, <https://doi.org/10.1175/JCLI-D-20-0517.1>.
- Steiner, M. R., R. A. Houze Jr., and S. E. Yuter, 1995: Climatological characterization of three-dimensional storm structure from operational radar and rain gauge data. *J. Appl. Meteor.*, **34**, 1978–2007, [https://doi.org/10.1175/1520-0450\(1995\)034<1978:CCOTDS>2.0.CO;2](https://doi.org/10.1175/1520-0450(1995)034<1978:CCOTDS>2.0.CO;2).
- Steranka, J., E. Rodgers, and R. C. Gentry, 1977: The diurnal variation of Atlantic Ocean tropical cyclone cloud distribution inferred from geostationary satellite infrared measurements. *Mon. Wea. Rev.*, **112**, 2338–2344, [https://doi.org/10.1175/1520-0493\(1984\)112<2338:TDVOAO>2.0.CO;2](https://doi.org/10.1175/1520-0493(1984)112<2338:TDVOAO>2.0.CO;2).
- Stevenson, S. N., K. L. Corbosiero, and S. F. Abarca, 2016: Lightning in eastern North Pacific tropical cyclones: A comparison to the North Atlantic. *Mon. Wea. Rev.*, **144**, 225–239, <https://doi.org/10.1175/MWR-D-15-0276.1>.
- Sundqvist, H., 1970: Numerical simulation of the development of tropical cyclones with a ten-level model. Part II. *Tellus*, **22**, 504–510, <https://doi.org/10.1111/j.2153-3490.1970.tb00516.x>.
- Tang, X., and F. Zhang, 2016: Impacts of the diurnal radiation cycle on the formation, intensity, and structure of Hurricane Edouard (2014). *J. Atmos. Sci.*, **73**, 2871–2892, <https://doi.org/10.1175/JAS-D-15-0283.1>.
- , Z. Tan, J. Fang, Q. Sun, and F. Zhang, 2017: Impacts of diurnal radiation cycle on secondary eyewall formation. *J. Atmos. Sci.*, **74**, 3079–3098, <https://doi.org/10.1175/JAS-D-17-0020.1>.
- Thompson, E. J., J. N. Moum, C. W. Fairall, and S. A. Rutledge, 2019: Wind limits on rain layers and diurnal warm layers. *J. Geophys. Res. Oceans*, **124**, 897–924, <https://doi.org/10.1029/2018JC014130>.
- Trabing, B. C., and M. M. Bell, 2021: The sensitivity of eyewall replacement cycles to shortwave radiation. *J. Geophys. Res. Atmos.*, **126**, e2020JD034016, <https://doi.org/10.1029/2020JD034016>.
- , —, and B. R. Brown, 2019: Impacts of radiation and upper tropospheric temperatures on tropical cyclone structure and intensity. *J. Atmos. Sci.*, **76**, 135–153, <https://doi.org/10.1175/JAS-D-18-0165.1>.
- Wang, Y.-F., and Z.-M. Tan, 2020: Outer rainbands-driven secondary eyewall formation of tropical cyclones. *J. Atmos. Sci.*, **77**, 2217–2236, <https://doi.org/10.1175/JAS-D-19-0304.1>.
- WMO, 1957: Definition of the tropopause. *WMO Bull.*, **6**, 136.

- Wu, Q., and Z. Ruan, 2016: Diurnal variations of the areas and temperatures in tropical cyclone clouds. *Quart. J. Roy. Meteor. Soc.*, **142**, 2788–2796, <https://doi.org/10.1002/qj.2868>.
- , J. Hong, and Z. Ruan, 2020: Diurnal variations in tropical cyclone intensification. *Geophys. Res. Lett.*, **47**, e2020GL090397, <https://doi.org/10.1029/2020GL090397>.
- Xu, K.-M., and D. A. Randall, 1995: Impact of interactive radiative transfer on the macroscopic behavior of cumulus ensembles. Part II: Mechanisms for cloud-radiation interactions. *J. Atmos. Sci.*, **52**, 800–817, [https://doi.org/10.1175/1520-0469\(1995\)052<0800:IOIRTO>2.0.CO;2](https://doi.org/10.1175/1520-0469(1995)052<0800:IOIRTO>2.0.CO;2).
- Yuter, S. E., and R. A. Houze, 1997: Measurements of raindrop size distributions over the Pacific warm pool and implications for $Z-R$ relations. *J. Appl. Meteor.*, **36**, 847–867, [https://doi.org/10.1175/1520-0450\(1997\)036<0847:MORSDO>2.0.CO;2](https://doi.org/10.1175/1520-0450(1997)036<0847:MORSDO>2.0.CO;2).
- Zhou, S., Y. Ma, and X. Ge, 2016: Impacts of the diurnal cycle of solar radiation on spiral rainbands. *Adv. Atmos. Sci.*, **33**, 1085–1095, <https://doi.org/10.1007/s00376-016-5229-5>.
- Zhu, T., and D.-L. Zhang, 2006: Numerical simulation of Hurricane Bonnie (1998). Part II: Sensitivity to varying cloud microphysical processes. *J. Atmos. Sci.*, **63**, 109–126, <https://doi.org/10.1175/JAS3599.1>.